

AD-A185 175

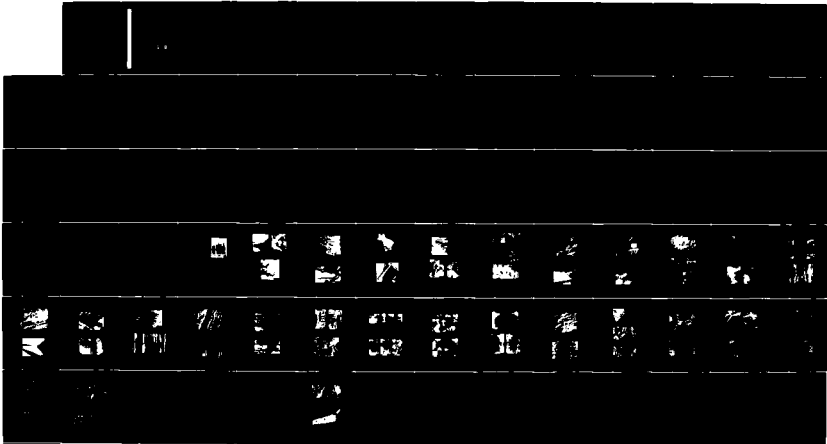
ENVIRONMENTALLY ASSISTED CRACKING: OVERVIEW OF EVIDENCE  
FOR AN ADSORPTION-INDUCED LOCALISED-SLIP PROCESS (U)  
AERONAUTICAL RESEARCH LABS MELBOURNE (AUSTRALIA)

1/1

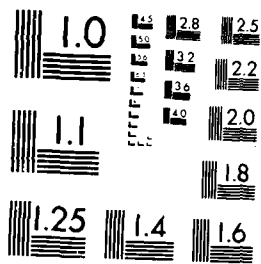
UNCLASSIFIED

S P LYNCH DEC 86 ARL/MAT-R-119

F/G 11/6.1 NL



END  
DATE  
FILMED  
11 87  
DTIC



MICROCOPY RESOLUTION TEST CHART  
NATIONAL BUREAU OF STANDARDS-1963-A

DTIC FILE COPY

13

ARL-MAT-R-119

AR-004-516



AD-A185 175

DEPARTMENT OF DEFENCE  
DEFENCE SCIENCE AND TECHNOLOGY ORGANISATION  
AERONAUTICAL RESEARCH LABORATORIES  
MELBOURNE, VICTORIA

Aircraft Materials Report 119

ENVIRONMENTALLY ASSISTED CRACKING :  
OVERVIEW OF EVIDENCE FOR AN ADSORPTION-INDUCED  
LOCALISED-SLIP PROCESS (U)

by  
S.P. Lynch

DTIC  
ELECTE  
SEP 28 1987  
S D

Approved for Public Release

(C) COMMONWEALTH OF AUSTRALIA 1986

DECEMBER 1986

87

3

AR-004-516

DEPARTMENT OF DEFENCE  
DEFENCE SCIENCE AND TECHNOLOGY ORGANISATION  
AERONAUTICAL RESEARCH LABORATORIES

Aircraft Materials Report 119

**ENVIRONMENTALLY ASSISTED CRACKING:  
OVERVIEW OF EVIDENCE FOR AN ADSORPTION-INDUCED  
LOCALISED-SLIP PROCESS**

by

S. P. LYNCH

SUMMARY

Metallographic and fractographic studies of crack growth in aluminium alloys, nickel, magnesium, titanium alloys B-brass iron-silicon, and high-strength steels in liquid-metal, aqueous, hydrogen, and inert environments are reviewed.



(C) COMMONWEALTH OF AUSTRALIA 1986

Accession For	
NTIS CRA&I	<input checked="" type="checkbox"/>
DTIC TAB	<input type="checkbox"/>
Unannounced	<input type="checkbox"/>
Justification	
By	
Date	
Author	
Dept	
Dist	

A-1

POSTAL ADDRESS: Director, Aeronautical Research Laboratories,  
P.O. Box 4331, Melbourne, Victoria, 3001, Australia.



**ENVIRONMENTALLY ASSISTED CRACKING:  
OVERVIEW OF EVIDENCE FOR AN ADSORPTION-INDUCED LOCALISED-SLIP PROCESS**

**ABSTRACT**

Metallographic and fractographic studies of crack growth in aluminium alloys, nickel, magnesium, titanium alloys,  $\beta$ -brass, iron-silicon, and high-strength steels in liquid-metal, aqueous, hydrogen, and inert environments are reviewed. Studies of transcrystalline cracking in single crystals are emphasised but some observations of intercrystalline cracking are also included. Remarkable similarities between hydrogen-assisted cracking, stress-corrosion cracking, and adsorption-induced liquid-metal embrittlement were observed for all the above materials. For a given material, not only was the detailed appearance of fracture surfaces similar but the crystallographic fracture planes and directions, and the active slip planes, were also the same for crack growth in the different embrittling environments. These and other similarities suggest that hydrogen-assisted cracking and stress-corrosion cracking as well as liquid-metal embrittlement are due to adsorption at crack tips for the materials and conditions studied. Embrittlement of aluminium alloys, nickel, titanium alloys, and magnesium in aqueous or hydrogen environments was also observed at such high crack velocities (under certain conditions) that there was insufficient time for diffusion of hydrogen ahead of cracks, further supporting a mechanism based on adsorption (of hydrogen) at crack tips. The metallographic and fractographic observations showed that environmentally assisted cracking occurred by a more localised plastic-flow/microvoid-coalescence process than that which occurred in inert environments. Dislocation processes occurring during ductile and brittle fracture are discussed, and it is concluded that environmentally assisted cracking occurs because adsorption facilitates the injection of dislocations from crack tips and thereby promotes the coalescence of cracks with voids ahead of cracks. Recent high-voltage transmission-electron microscopy studies, surface-science observations, and theoretical work, which support an adsorption mechanism or a localised-slip mechanism (or both) for environmentally assisted cracking, are also reviewed.

## CONTENTS

	Page No.
1. INTRODUCTION	1
2. EXPERIMENTAL PROCEDURE	3
3. COMPARISONS OF HYDROGEN-ASSISTED CRACKING AND STRESS-CORROSION CRACKING WITH ADSORPTION-INDUCED LIQUID-METAL EMBRITTLEMENT- TRANSCRYSTALLINE CRACKING	4
3.1 Aluminium and Al-Zn-Mg Single Crystals	4
3.1.1 LME	4
3.1.2 Rapid Fracture in Aqueous Environments	5
3.1.3 Slow SCC	6
3.2 Nickel Single Crystals	7
3.3 Fe-Si Single Crystals	8
3.4 $\beta$ -Brass Single Crystals	8
3.5 Pure Magnesium	9
3.6 $\alpha$ -Titanium Alloys	10
4. COMPARISONS OF HYDROGEN-ASSISTED CRACKING AND STRESS-CORROSION CRACKING WITH ADSORPTION-INDUCED LIQUID-METAL EMBRITTLEMENT - INTERCRYSTALLINE CRACKING	10
4.1 Aluminium Alloys	10
4.2 Pure Magnesium	11
4.3 High-Strength Steel (D6ac)	11
5. DISCUSSION	12
5.1 Evidence for an Adsorption Mechanism for Hydrogen-Assisted Cracking and Stress-Corrosion Cracking	12
5.1.1 Similarities between HAC/SCC and LME	12
5.1.2 HAC/SCC at High Velocities	12
5.1.3 Absence of an Effect of Solute Hydrogen on Fracture	15
5.2 Evidence for a Localised-Slip Mechanism for Environmentally Assisted Cracking	16
5.2.1 Metallographic and Fractographic Observations	16
5.3 Dislocation Activity During Ductile and 'Brittle' Crack Growth	18
5.3.1 Ductile Crack Growth	18
5.3.2 Brittle Crack Growth	19
5.4 Other Evidence for a Localised-Slip/Adsorption Mechanism	21
5.4.1 In-situ High-Voltage TEM Fracture Studies	21
5.4.2 Surface Science Observations and Theoretical Considerations	23
6. CONCLUDING REMARKS	25
ACKNOWLEDGEMENTS	
REFERENCES	
APPENDIX	
FIGURES	
DISTRIBUTION LIST	

## 1. INTRODUCTION

The resistance of many materials to the initiation and growth of cracks is often substantially lower in liquid-metal, aqueous, and hydrogen environments than in inert environments [1-8]. This effect is known in general terms as environmentally assisted cracking and, for specific environments, is known as liquid-metal embrittlement (LME), stress-corrosion cracking (SCC), and hydrogen-assisted cracking (HAC). LME is undoubtedly the most dramatic of these processes, with crack growth in liquid-metal environments occurring at velocities as high as ~100 mm/s at stress-intensity factors,  $K$ , as low as ~10% of the critical  $K$  for fracture in inert environments (Fig. 1) [9,10]. Moreover, LME can produce cleavage-like fractures in metals which would normally fail by ductile rupture in air (Fig. 2) [11-15].

LME does not occur for all combinations of solid and liquid metals (Appendix I) [16] but the reasons for this 'specificity' are not well understood. However, as a general guideline, LME is likely to occur when there are limited mutual solubilities and little tendency to form intermetallic compounds between solid and liquid metals [13-16]. Solid-metal and metal-vapour environments can also produce embrittlement but crack growth is slower in these environments than in liquid-metal environments since surface-diffusion and vapour-transport of metal atoms to crack tips are much slower than capillary-flow of liquid metals to crack tips.

It is generally accepted [11-15] that rapid fracture in embrittling liquid-metal environments is caused by **adsorption** of environmental-metal atoms at crack tips since there is neither the tendency nor the time for other reactions to occur.† Workers studying LME in the 1960's and early 1970's [11-13, 17] concluded that adsorption lowered the stress required

---

†There are some liquid-solid metal couples where either diffusion of embrittling atoms along grain boundaries or other reactions during pre-exposure of unstressed specimens can lead to subsequent embrittlement [15] but none of the examples of LME considered in the present report fall into this category.

(2)

for tensile separation of atoms ('decohesion') at crack tips, but did not affect the stress required for slip around crack tips, so that (i) decohesion in intrinsically brittle materials such as zinc single crystals occurred at lower stresses in liquid-metal environments than in air, and (ii) decohesion occurred in preference to slip in normally ductile materials such as aluminium single crystals tested in liquid-metal environments. However, detailed metallographic and fractographic observations to substantiate this mechanism were not made during these early studies. Subsequent observations supported a decohesion process for LME in zinc [18] but indicated that LME of aluminium and other ductile materials occurred by an adsorption-induced localised-slip process [18-21].

Similarities between LME and HAC/SCC were observed as long ago as 1874 by Johnson [22] who noted that the embrittlement of steel by hydrogen and by liquid zinc had some common characteristics! More recently, the similar effects of microstructure (e.g. grain size, extent of cold working), grain-boundary segregation, yield strength, slip mode, temperature, and other variables on the degree of embrittlement produced by aqueous, hydrogen, and liquid-metal environments have been reported by a number of workers [14, 19, 23-28]. The form of crack-velocity versus stress-intensity factor ( $v$ - $K$ ) plots is also similar for HAC, SCC, and LME, with a strong dependence of  $v$  on  $K$  at low  $K$ , and little or no dependence of  $v$  on  $K$  at high  $K$  (Fig. 1). The propensity for brittle intercrystalline cracking in aqueous, hydrogen, and liquid-metal environments has also been noted on numerous occasions [23-27].

The above similarities between LME, SCC, and HAC led a number of workers to suggest that these processes occurred by a common mechanism [23-27]. However, this idea was not widely accepted since it was argued that the similarities could be explained in other ways. For example, embrittlement would generally be greater in higher strength materials regardless of the mechanism of crack growth since most fracture processes occur more readily when less plastic relaxation (blunting) occurs at crack tips. Similarly, featureless intercrystalline fracture surfaces could be produced by adsorption-induced fracture, fracture of thin hydride films at grain boundaries, or localised dissolution. In other words, the

similarities between HAC, SCC, and LME listed above, are not by themselves convincing evidence for a common mechanism although, of course, they are consistent with one.

The remarkable metallographic and fractographic similarities between LME, SCC, and HAC, when there are distinctive slip distributions around cracks and when fracture surfaces exhibit distinctive features, on the other hand, are more persuasive that the same mechanism is applicable to all these processes [28-36]. Observations of embrittlement in aqueous and hydrogen environments at high crack velocities, and other considerations, also suggest that adsorption is responsible for SCC and HAC as well as for LME [28-35]. In the present report, these observations for aluminium alloys [28-31], nickel [32], magnesium [33, 34], titanium alloys [28], and high-strength steels [36], are reviewed. Some unpublished work [35] for these materials and for Fe-Si and  $\beta$ -brass is also summarised. Comparisons of LME, SCC and HAC in single crystals are emphasised since the appearance of fracture surfaces is generally uniform, and crystallographic fracture planes, crack directions, and active slip planes are easily determined in single crystals. An adsorption-induced localised-slip process which accounts for the observations is then discussed.

## 2. EXPERIMENTAL PROCEDURE

Only a brief description of the experimental techniques is given here — further details for particular materials can be found in the references cited in the respective sections. Single-crystals (notched along one edge) or material with large (10-20 mm) grain sizes (notched along one edge so that crack growth occurred within a single grain) were used to study crack growth in many of the materials. Specimens were generally fatigue-precracked, and then tested in cantilever bending under either sustained or dynamic loading; for the latter, deflection rates of 0.0006°/s up to 60°/s were used. The high deflection rates were used to determine whether environmentally assisted cracking could occur at very high crack velocities. For commercial alloys, bolt-loaded double-cantilever-beam specimens were tested under sustained loading.

Scanning-electron microscopy (SEM) and transmission-electron microscopy (TEM) of secondary-carbon replicas were used to study fracture surfaces. Replicas were prepared and examined under optimum conditions [37, 38] (Fig. 3) in order to resolve smaller, shallower features than could be detected by SEM. Prior to examination of LME fractures, liquid or solid metals were removed from fracture surfaces as follows: Mercury was evaporated from fractures in a vacuum at  $-100^{\circ}\text{C}$ , alkali metals were dissolved in alcohols, a low-melting-point ( $47^{\circ}\text{C}$ ) bismuth alloy (44.7%Bi 22.6%Pb 19.1%In 8.3%Sn 5.3%Cd) (on aluminium) was dissolved in concentrated nitric acid (which does not attack aluminium), and gallium was removed by stripping plastic replicas from fractures.

### 3. COMPARISONS OF HYDROGEN-ASSISTED CRACKING AND STRESS-CORROSION CRACKING WITH ADSORPTION-INDUCED LIQUID-METAL EMBRITTLEMENT -- TRANSCRYSTALLINE CRACKING

#### 3.1 Aluminium and Al-Zn-Mg Single Crystals [19-21, 29, 30, 35]

##### 3.1.1 LME

Aluminium single crystals ( $\sim 99.99\%$  purity) cracked in liquid-metal environments exhibited cleavage-like fracture surfaces macroscopically parallel to  $\{100\}$  planes (Fig. 2). Unlike classical cleavage cracks, crack-tip-opening angles were large ( $\sim 10-20^{\circ}$ ), extensive slip occurred around cracks, especially on  $\{111\}$  planes intersecting crack tips, and dislocation-cell structures were observed just beneath fracture surfaces (Fig. 4). Furthermore, crack fronts were parallel to  $\langle 110 \rangle$  directions, i.e. parallel to the line of intersection of slip planes with the crack plane, and slip lines parallel to crack fronts were observed on fracture surfaces. For many crystal orientations, crack growth occurred in **two**  $\langle 110 \rangle$  directions so that crack fronts were a V-shape or zig-zag shape (Fig. 5). Examination of fracture surfaces at high magnifications showed that they were microscopically dimpled (Figs 6, 7), indicating that crack growth involved the nucleation and growth of voids ahead of crack tips.

LME in high-purity Al 6%Zn 3%Mg single crystals also produced  $\{100\}$  cleavage-like fracture surfaces with crack growth in  $\langle 110 \rangle$  directions for all crystal orientations. Furthermore, the slip distribution and approximate strains around cleavage-like  $\{100\}$  cracks could be determined

in the interior of specimens by ageing after crack growth (to 'decorate' dislocations), then sectioning, polishing, and etching. The slip distribution in specimen interiors was similar to that on the side surface of specimens, and considerable slip on planes intersecting crack fronts was observed (Fig. 8). Electron-channelling patterns from fracture surfaces could not be obtained and Laue X-ray back-reflection spots from fracture surfaces were severely distorted, further confirming that large strains were associated with crack growth.

The degree of embrittlement in Al-Zn-Mg was greater than that in pure aluminium, and increased with increasing strength produced by precipitation-hardening; greater degrees of embrittlement were characterised by smaller crack-tip-opening angles and more-localised slip around crack tips (Figs 8,9). Furthermore, the size of dimples on fracture surfaces increased with increasing degree of overaging — consistent with dimples resulting from formation of voids around ageing precipitates ahead of cracks. Crack growth in inert environments also involved void formation around ageing precipitates (and around more widely spaced inclusions) but the appearance of fracture surfaces produced by LME and by overload in air was quite different. At low magnifications, LME fractures were cleavage-like whereas overload fractures were covered with large, deep dimples; at high magnifications, small, shallow dimples were observed on {100} cleavage-like facets while small, stretched dimples within large, deep dimples were observed on overload fractures (Fig. 10).

### 3.1.2 Rapid Fracture in Aqueous Environments

Cleavage-like fracture surfaces macroscopically parallel to {100} planes with crack growth in  $\langle 110 \rangle$  directions were also produced by fracture of precipitation-hardened Al-Zn-Mg single crystals in aqueous environments — even at crack velocities as high as 10 mm/s produced by rapid dynamic loading (Fig. 11a). The detailed appearance of cleavage-like fracture surfaces produced in aqueous environments was also similar to that produced by LME in that dimples, whose size and spacing depended on the ageing conditions, were observed.

For an overaged condition (HV-100 - the minimum Vickers hardness at which embrittlement occurred during rapid cracking in water), small dimples associated with ageing precipitates could be faintly resolved on fracture surfaces by SEM (Fig. 11b) but were more clearly apparent on TEM micrographs (Figs 11c,d). Many Y-shaped ridges, which match peak-to-peak on opposite fracture surfaces and 'point' in the direction of crack growth, were also observed on fracture surfaces of overaged specimens. These ridges were produced when cracks intersected larger-than-average voids nucleated by small inclusions ahead of cracks, although the 'leading' edge of the dimple, and inclusion within the dimple, were only clearly visible in some cases (Fig. 11c). For peak-aged specimens (HV -160) cracked rapidly in water, isolated large dimples associated with inclusions were observed on cleavage-like fracture surfaces by SEM (Fig. 12a), but TEM of replicas was necessary to resolve extremely small depressions which were probably dimples associated with larger-than-average ageing precipitates (Fig. 12b).

Crack-tip-opening angles produced by rapid fracture in water were larger than those produced by LME (for equivalent ageing conditions) but the distribution of slip around cracks was similar, with slip occurring particularly on planes intersecting crack fronts (Fig. 13). Laue X-ray back-reflection spots from fracture surfaces were extremely diffuse, confirming that crack growth was associated with large, localised strains.

### 3.1.3 Slow SCC

Sustained-load cracking of peak-aged (HV -160) Al-Zn-Mg single crystals at high K in distilled water and moist-air (20% relative humidity) environments occurred at crack velocities  $10^{-3}$  mm/s and  $10^{-7}$  mm/s, respectively. Cleavage-like {100} <110> fracture surfaces, covered with isolated large dimples and extremely small dimples, similar to those produced by rapid fracture in aqueous and liquid-metal environments were observed after slow SCC (Fig. 14). Crack-arrest markings, which are indicative of discontinuous cracking, were **not** observed. There were also no signs that significant dissolution had occurred during SCC. Crack-tip-opening angles produced by slow SCC were much smaller than those produced by rapid fracture in water but the

distribution of slip around cracks was similar, with slip occurring particularly on planes intersecting crack fronts (Fig. 15).

### 3.2 Nickel Single Crystals [32, 35]

Embrittlement of nickel single crystals (~99.5% purity) in gaseous hydrogen environments under rapid dynamic loading was observed at crack velocities as high as ~1 mm/s. Under these conditions, the appearance of fracture surfaces was identical to that produced by rapid fracture (~1 mm/s) in liquid mercury. Furthermore, the appearance of fractures depended somewhat on the orientation of crystals but was the same in hydrogen and mercury environments for each orientation. For crystals with specimen axes near  $\langle 100 \rangle$ , fracture planes were approximately parallel  $\{100\}$  planes, with crack growth in  $\langle 110 \rangle$  directions, whereas for orientations such that  $\{100\}$  planes were steeply inclined to specimen axes, deviations of up to  $-25^\circ$  from  $\{100\}$  planes and a higher density of steps were observed (Figs 16 - 18).

The degree of embrittlement produced by rapid cracking (~1 mm/s) in gaseous hydrogen (101kPa) and liquid mercury was also approximately the same, with crack-tip-opening angles  $\sim 45^\circ$ . However, embrittlement in hydrogen was greater at lower crack velocities (crack-tip opening angles for HAC were  $\sim 30^\circ$  for crack velocities  $\sim 10^{-3}$  mm/s) whereas embrittlement in mercury was not affected by crack velocity.† Fracture surfaces produced by slow crack growth in hydrogen (Fig. 19a) were similar to those produced by rapid cracking except that there were fewer coarse slip lines (produced by slip behind crack tips), and more steps and Y-shaped ridges, for the former.

TEM of replicas of fracture surfaces revealed that the areas between the tear ridges and coarse slip bands had a 'rumpled' appearance due to

---

†The degree of embrittlement probably decreases with increasing crack velocity for HAC but not for LME because gaseous diffusion of hydrogen is much slower than capillary flow of liquid metals to crack tips. The surface coverage of adsorbed atoms at crack tips, which probably determines the degree of embrittlement, therefore decreases with increasing velocity for HAC but not for LME.

the presence of fine slip traces and very small depressions (Fig. 19b). Laue X-ray back-reflection patterns could not be obtained from fracture surfaces showing that strains beneath fracture surfaces were very large. Extensive plastic zones, with slip occurring particularly on planes intersecting crack fronts, were also observed on the side surfaces of specimens after both HAC and LME (Fig. 20).

### 3.3 Fe-Si Single Crystals [35]

The degree of embrittlement of Fe 2.6%Si single crystals in gaseous hydrogen environments depends on the hydrogen pressure, temperature, and strain rate [39]. Environmental effects at ambient temperature are only observed at low crack velocities since high strain rates induce extremely rapid unstable fracture. For crack growth in gaseous hydrogen (101kPa) at 25°C at a crack velocity  $\sim 10^{-3}$  mm/s, the crack-tip-opening angle ( $\sim 8^\circ$ ) was approximately the same as that produced by rapid crack growth ( $\sim 1$ mm/s) in liquid indium at 160°C and liquid lithium at 210°C, and fracture surfaces produced by HAC and LME were essentially the same (Fig. 21). Fracture surfaces were macroscopically parallel to {100} planes with crack growth in  $\langle 110 \rangle$  directions, and steps parallel to these directions formed herringbone patterns similar to those observed for Al-Zn-Mg and nickel. Crack growth in dry air, under equivalent testing conditions to those used for hydrogen and liquid-metal environments, produced ductile fractures.

Examination of cleavage-like fracture surfaces at high magnifications by SEM showed ragged steps, tear ridges, slivers of material projecting from the fracture surfaces, and isolated small dimples (Fig. 21b,d). TEM of replicas of fracture surfaces revealed closely spaced slip lines and small depressions between the tear ridges and steps (Fig. 22). Electron-channelling patterns from fracture surfaces could not be obtained showing that strains just beneath fracture surfaces were at least  $\sim 10\%$ . Extensive slip, particularly on {112} planes intersecting crack fronts, was observed on specimen side surfaces after crack growth in hydrogen and liquid-metal environments (Fig. 23).

### 3.4 $\beta$ -Brass Single Crystals [35]

For  $\beta$ -brass (48.8%Zn 51.2%Cu) single crystals, cleavage-like {100} fracture surfaces were observed after rapid crack growth ( $>10$  mm/s) in

liquid gallium and slow crack growth ( $\sim 10^{-4}$  mm/s) in distilled water. Crack growth occurred in two  $\langle 110 \rangle$  directions so that herringbone patterns, similar to those observed for Al-Zn-Mg, nickel, and Fe-Si, were produced (Fig. 24). Detailed observations of fracture surfaces and of slip distributions around cracks were not made, but slip lines parallel to crack fronts were observed on fracture surfaces, and Laue X-ray back-reflection spots from fracture surfaces were diffuse, showing that appreciable, localised strains were associated with crack growth.

### 3.5 Pure Magnesium [33,34]

Environmentally assisted cracking in magnesium crystals (99.99% purity), occurred at crack velocities as high as  $\sim 50$  mm/s in aqueous environments under dynamic loading. 'Brittle' fracture surfaces macroscopically parallel to pyramidal planes of the type  $\{10\bar{1}X\}$  (where X was commonly 1) were observed after crack growth in aqueous and inert environments but the detailed appearance of fracture surfaces produced in inert and embrittling environments was significantly different. Fracture in dry air produced deep flutes (elongated dimples) with more equiaxed dimples within the flutes, while rapid fracture in an aqueous environment produced shallow flutes containing very small dimples. Cleavage-like facets and secondary cracks parallel to basal planes were also observed after rapid fracture in aqueous environments but not after fracture in dry air. River lines, twin traces, and tongues produced by crack growth along twin/matrix interfaces, were observed on basal-plane facets (Figs 25,26).

Fluted fracture surfaces parallel to pyramidal planes, and basal cleavage-like facets, were also produced by slow crack growth in aqueous environments and by rapid fracture in liquid-metal environments (Na, K, Rb, Cs). Fracture surfaces were similar to those produced by rapid fracture in aqueous environments except that (i) flutes were smaller and shallower, and (ii) twin traces and tongues on basal facets were fewer, after rapid LME and slow SCC (Figs 27, 28).

---

<sup>t</sup>Flutes are produced by the coalescence of tubular voids which nucleate along slip-band intersections ahead of cracks [33, 40, 41].

### 3.6 $\alpha$ -Titanium Alloys [28,35]

SCC of titanium alloys in aqueous environments can also occur at high crack velocities, although not as high as observed for Al-Zn-Mg and magnesium, nor as high as for LME. The 'plateau' crack velocity at high stress-intensity factors in a mill-annealed Ti 8%Al 1%Mo 1%V alloy in a 10M HCl environment is  $\sim 0.4$  mm/s — approximately two orders of magnitude lower than the plateau velocity in liquid mercury (Fig. 1) [9]. Embrittlement of a mill-annealed Ti 6%Al 4%V alloy in an HCl + NaCl environment under dynamic loading was also observed at crack velocities up to  $\sim 0.4$  mm/s [35]. SCC of a Ti 6%Al 0.3% O alloy in a KCl solution at a velocity  $\sim 3$  mm/s has also been reported [9]. Cleavage-like fracture surfaces parallel to basal planes (or possibly  $10-17^\circ$  from basal planes [42]), and fluted regions roughly perpendicular to cleavage facets, were produced by SCC at both high and low crack velocities and by rapid cracking in liquid mercury (Fig. 29). Overload fractures in dry air were completely covered with equiaxed dimples. At high magnifications, tear ridges and small, shallow dimples were observed on cleavage-like facets (Fig. 30).

## 4. COMPARISONS OF HYDROGEN-ASSISTED CRACKING AND STRESS-CORROSION CRACKING WITH ADSORPTION-INDUCED LIQUID-METAL EMBRITTLEMENT — INTERCRYSTALLINE CRACKING

### 4.1 Aluminium Alloys [31,35]

Intercrystalline fracture surfaces, produced by rapid cracking ( $\sim 10$  mm/s) in liquid-metal environments and by slow SCC ( $\sim 10^{-4}$  mm/s) in aqueous and moist-air environments in Al 6%Zn 3%Mg bicrystals with 'wide' precipitate-free zones (PFZ) at grain boundaries, were covered with small, shallow dimples; intercrystalline fractures produced in dry air were covered with large, deep dimples with small dimples within them (Figs 31, 32). Striations (crack-arrest markings) were sometimes observed on fracture surfaces produced by SCC (but not by LME) suggesting that SCC was sometimes discontinuous. Intercrystalline fracture surfaces produced by sub-critical cracking in Al-Zn-Mg bicrystals with narrow PFZ, and in commercial 7075-T651 aluminium alloys, in liquid/solid metal and

aqueous/moist-air environments were relatively smooth, although isolated areas of dimples and tear ridges were evident (Fig. 33).

#### 4.2 Pure Magnesium [33,34]

Environmentally assisted intercrystalline cracking, like transcrystalline cracking, was observed at crack velocities as high as ~50 mm/s in aqueous environments. Specimens partially cracked in aqueous environments and then cracked in dry air under dynamic loading showed transitions from 'brittle' to 'ductile' intercrystalline fracture surfaces similar to those observed for Al-Zn-Mg. Examination of 'brittle' regions at high magnifications by SEM revealed small, shallow dimples in some areas while other areas appeared relatively smooth except for fine slip and twin traces; 'ductile' regions were covered with large, deep dimples with smaller, shallower dimples within them (Fig. 34). TEM of replicas showed that the 'smooth' areas observed by SEM on 'brittle' fractures were covered with shallow flutes, small dimples, and closely spaced slip lines (Fig. 35). Brittle intercrystalline fractures were also produced by slow crack growth in aqueous environments and by rapid cracking in liquid-metal environments (Na, K, Rb, Cs), and small, shallow dimples were evident in some areas at high magnifications (Fig. 36).

#### 4.3 High-Strength Steel (D6ac) [36]

The fracture path and appearance produced by HAC and LME in D6ac steel (0.46%C 1.2%Mo 1.1%Cr 0.12%V 0.8%Mn 0.24%Si 0.004%P 0.002%S), heat-treated to produce a lath-type, tempered-martensitic structure, depended on the tempering temperature. Nevertheless, the fracture path and appearance after sub-critical cracking in gaseous hydrogen (101kPa) and liquid mercury environments were similar for each tempering temperature. For example, specimens austenitised, step-quenched, and double-tempered for 1 + 1 h at (i) 290°C, (ii) 400°C, and (iii) 650°C, and then cracked in hydrogen and mercury environments, exhibited (i) dimpled fractures predominately along martensite - lath boundaries (Fig. 37), (ii) 'brittle' intercrystalline fractures along prior-austenite grain boundaries (Fig. 38), and (iii) dimpled intercrystalline fractures along prior-austenite grain boundaries (Figs 39, 40), respectively. Overload fractures produced

in dry air were transcrystalline and dimpled for all tempering temperatures; dimples were generally larger and deeper than those observed after HAC and LME, although small dimples within large dimples, were observed on overload fractures. The change in fracture path and appearance with specimen tempering temperature for HAC and LME is largely associated with the segregation of embrittling elements such as phosphorus to prior-austenite grain boundaries during tempering in the range 350° - 650°C and there appears to be a similar interaction between grain-boundary segregants and hydrogen, and between segregants and mercury.

## **5. DISCUSSION**

### **5.1 Evidence for an Adsorption Mechanism for Hydrogen-Assisted Cracking and Stress-Corrosion Cracking**

#### **5.1.1 Similarities between HAC/SCC and LME**

The remarkable metallographic and fractographic similarities between LME, SCC, and HAC obviously suggest that the mechanism of embrittlement is the same for the materials and testing conditions studied : Different mechanisms of crack growth are unlikely to produce fractures with the same crystallographic fracture plane, same crystallographic direction of crack growth, same distribution of slip around crack tips, and same fine details (e.g. dimples, tear ridges, slip lines) on fracture surfaces, as was observed. The fact that such similarities occur in a wide variety of materials (fcc, bcc, and hcp) which fail by a number of different fracture modes is also striking. The similar effects of microstructure, strength, slip mode, and other variables on HAC/SCC and LME are also consistent with a common mechanism, as mentioned in the introduction. Thus, these observations suggest that adsorbed hydrogen atoms, produced by dissociation of water or hydrogen molecules, are responsible for HAC and SCC in the same way as adsorbed metal atoms are responsible for LME.

#### **5.1.2 HAC/SCC at High Velocities**

Observations that HAC/SCC can occur at high velocities in materials with low hydrogen diffusivities demonstrate that adsorbed hydrogen can produce HAC/SCC. The distance that hydrogen adsorbed at crack tips can diffuse ahead of growing cracks has been calculated [43] using the

equation  $C/C_0 = \text{erfc}(vx/D)^{1/2}$ , where  $C_0$  is the concentration of hydrogen at the crack tip,  $C$  is the hydrogen concentration a distance  $x$  ahead of the crack along its line of prolongation,  $v$  is the steady state crack velocity, and  $D$  is the diffusivity of hydrogen. For  $C/C_0 \sim 0.1$ ,  $x \approx D/v$ , and for  $C/C_0 \sim 0.005$ ,  $x \approx 4D/v$ . Interatomic distances are  $\sim 3 \times 10^{-8}$  cm and, hence, this analysis shows that there should not be significant hydrogen diffusion ahead of cracks for  $D/v$  ratios of less than  $\sim 10^{-8}$  cm, as is the case for environmentally assisted cracking at the maximum observed velocities for magnesium, Al-Zn-Mg, nickel, and  $\alpha$ -titanium alloys (Table I). For steels (with  $D \sim 10^{-6}$  cm<sup>2</sup>/s), diffusion will produce a hydrogen concentration of  $0.5C_0$  at a distance of about 10 atomic spacings ahead of cracks moving at 1 cm/s.

TABLE I  
Maximum Observed Crack Velocities,  $v$ , for Environmentally Assisted Cracking and Hydrogen Diffusivities,  $D$ , for Various Materials and Environments at 20-25°C [34].

Material:Environment	$v$ (cm/s)	$D$ (cm <sup>2</sup> /s)	$D/v$ (cm)
Pure Mg : NaCl+K <sub>2</sub> CrO <sub>4</sub> solution	5 [33,34]	$\sim 10^{-9}$ [45]	$\sim 2 \times 10^{-10}$
Peak-aged Al-Zn-Mg : H <sub>2</sub> O	1 [29-31]	$\sim 10^{-10}$ [46,47]	$\sim 10^{-10}$
Martensitic steels : H <sub>2</sub> S(100kPa)	1 [44]	$10^{-5}$ - $10^{-8}$ [48]	$\leq 10^{-5}$
$\alpha$ - Ti alloy : KCl solution	0.3 [9]	$10^{-9}$ - $10^{-12}$ [49-52]	$\leq 10^{-8}$
Ni 200 : H <sub>2</sub> (100 kPa)	0.1 [32]	$2-5 \times 10^{-10}$ [53,54]	$\leq 5 \times 10^{-9}$

Hydrogen can be transported more rapidly by mobile dislocations than by lattice diffusion [55-57] but the initial velocity of dislocations injected from rapidly growing cracks (assuming that crack growth involves dislocation injection) is probably too high for atmospheres of hydrogen to form around dislocations. The velocity of dislocations injected from rapidly growing cracks is not known but should be at least as high as the crack velocity since dislocations nucleated at crack tips will be pushed into the material by succeeding dislocations nucleated at crack tips. For a dislocation velocity  $\sim 1$  cm/s, the time,  $t$ , for a dislocation to move one atomic distance,  $a$ , ahead of a crack is  $\sim 3 \times 10^{-8}$  s, and saturation of the

dislocation core would require a minimum diffusivity, ( $D=a^2/2t$ ),  $\sim 10^{-8}$  cm<sup>2</sup>/s [57]. Dislocation transport of hydrogen ahead of cracks would therefore not be expected during environmentally assisted cracking at the maximum velocities observed for magnesium, Al-Zn-Mg, nickel, and titanium alloys. Even if dislocation transport of hydrogen did occur, hydrogen would be swept along slip planes steeply inclined to crack planes and would not accumulate directly ahead of cracks unless hydrogen was subsequently transferred to other dislocations moving towards the region ahead of cracks.

The values of  $D$  (Table I) were generally obtained using polycrystalline specimens but reflect the rates of lattice diffusion since possibly faster diffusion along grain boundaries would generally not be detectable. Studies for nickel [59] suggested that grain-boundary diffusivities of hydrogen were up to one hundred times faster than lattice diffusivities but it is not known whether such an effect (and its magnitude) is a general one. Thus, diffusion of hydrogen ahead of rapidly growing intercrystalline cracks cannot be completely discounted. The values of  $D$  were also obtained using unstressed specimens but experimental data suggest that an elastic stress either has no effect on  $D$  [60] or produces only a small increase in  $D$  [61]. Theoretical studies also suggest that a hydrostatic stress **gradient** (and associated gradient in lattice dilatation) should not significantly increase  $D$  for fcc metals, although large increases would be expected for bcc metals [62].

Lattice spacings in the first few atomic layers at surfaces are sometimes different from bulk spacings due to the presence of the surface and adsorbed atoms at the surface (see 5.4.2). Whether such surface-lattice perturbations occur at growing crack tips and influence hydrogen diffusivities in the first few atomic layers is not known. However, the possible presence of hydrogen one or two atomic spacings beneath the surface, as well as at the surface, does not affect the conclusion that

---

†HAC in nickel has also been observed at temperatures as low as 77K where neither lattice diffusion nor dislocation transport ahead of cracks should have occurred [58].

HAC/SCC at the high crack velocities in Mg, Al-Zn-Mg, Ni, and Ti alloys must involve weakening of interatomic bonds at crack tips, as discussed in section 5.3.2.

### 5.1.3 Absence of an Effect of Solute Hydrogen on Fracture

The case for an adsorption mechanism for HAC/SCC at low velocities, when hydrogen undoubtedly does diffuse ahead of cracks, is supported not only by similarities between HAC/SCC at low and high velocities (and between SCC/HAC and LME) but also by observations which suggest that the presence of solute hydrogen does not produce embrittlement. For example, the presence of solute hydrogen can produce hardening or softening in iron and nickel depending on the material purity, temperature, and strain-rate [63,64] but HAC is observed regardless of which effect occurs, suggesting that HAC is **not** associated with the effects of solute hydrogen on dislocation activity ahead of cracks [32]. Furthermore, Al-Zn-Mg and nickel **single crystals**, thermally or cathodically charged with hydrogen and tested in air at slow strain rates so that hydrogen would be present as solute ahead of cracks but not adsorbed at (oxide covered) crack tips, exhibited ductile behaviour during fatigue precracking and subsequent overload fracture (Figs 41, 42) [29, 32].

The embrittlement observed in many hydrogen-charged materials tested in air at slow strain rates can be explained by diffusion or dislocation transport of hydrogen to, and **adsorption** at, internal cracks or interfaces. For example, such processes would account for the small areas of brittle cracking observed around large voids some distance ahead of fatigue precracks in hydrogen-charged nickel single crystals (Figs 43, 44) [32]. Hydrogen diffusion to, and adsorption at, internal cracks may also be necessary during SCC if hydrogen adsorption at external cracks is inhibited by oxide films. In such cases, crack growth may be discontinuous since crack growth may stop until sufficient hydrogen accumulates at internal cracks. Crack-arrest markings indicative of discontinuous cracking were sometimes observed on intercrystalline fracture surfaces produced by SCC in Al-Zn-Mg but were not detected on any of the other fracture surfaces examined.

Considering (i) the absence of an effect of solute hydrogen on fracture, (ii) the lack of evidence for hydride formation and localised dissolution (in the materials/environments where such reactions are possible), (iii) the observations of HAC/SCC at high velocities, and (iv) the similarities between HAC/SCC and adsorption - induced LME, there can be little doubt that hydrogen adsorbed at the tips of internal or external cracks is responsible for SCC and HAC for the materials and testing conditions studied.

## **5.2 Evidence for a Localised-Slip Mechanism for Environmentally Assisted Cracking**

### **5.2.1 Metallographic and Fractographic Observations**

Strains associated with environmentally induced 'brittle' fractures were smaller and more localised than those associated with ductile fractures. Nevertheless, slip occurred on planes intersecting crack fronts, strains just beneath fracture surfaces were substantial (generally at least -10%), and small, shallow dimples were generally observed on fracture surfaces produced by environmentally assisted cracking. Large, deep dimples, with small dimples within them, were generally observed on ductile fracture surfaces. These observations indicate that environmentally assisted cracking occurs by a more localised microvoid-coalescence process than that which occurs in inert environments - a conclusion first made by Beachem [66] some time ago for HAC in steels.

The fracture-surface dimples indicative of a microvoid-coalescence process for environmentally assisted cracking were sometimes clearly evident when fracture surfaces were examined by SEM at relatively low magnifications (<1,000X). In other cases, examination of fracture surfaces at high magnifications (>5,000X) by SEM was necessary to resolve small dimples, and often dimples were resolved only in some areas. In yet other cases, SEM examination at high magnifications revealed predominantly smooth areas except for isolated dimples and tear ridges. Examination of such 'smooth' areas by TEM of secondary-carbon replicas, shadowed at low angles and examined at high tilt angles (Fig. 3), showed they were often covered with small depressions and sometimes also by closely spaced slip lines.

For overaged Al-Zn-Mg single crystals cracked rapidly in aqueous environments (Fig. 11), the small depressions are undoubtedly dimples since there were a high density of incoherent precipitates (void nuclei) and high strains associated with crack growth. The extremely small depressions observed on cleavage-like fracture surface of peak-aged Al-Zn-Mg single crystals (Fig. 12), containing a finer dispersion of precipitates than overaged specimens, are therefore probably also dimples since the general characteristics of fracture were similar for overaged and peak-aged specimens. Accepting this, the observations for peak-aged specimens indicate that the microvoid-coalescence process can occur on such a localised scale that dimples can only just be resolved on fracture surfaces by TEM of replicas prepared and examined under optimum conditions — a procedure which is rarely used. The small depressions observed on other cleavage-like fracture surfaces are similar to those observed for Al-Zn-Mg and, hence, are probably also dimples, although voids are probably nucleated predominantly at dislocation-cell boundaries or slip-band intersections in materials not containing a high density of second-phase particles [67, 68].

Further evidence that the microvoid-coalescence process can sometimes occur on such a localised scale that dimples are difficult to resolve on fracture surfaces was obtained from studies of intercrystalline fracture of Al-Zn-Mg bicrystals in inert environments [31]. Fracture of specimens with 'wide' precipitate-free zones (PFZ) at grain boundaries produced large deep dimples on fracture surfaces, but decreasing the PFZ width, increasing the area fraction of grain-boundary precipitates, and increasing matrix strength, resulted in a progressive decrease in the size and depth of dimples on fracture surfaces until dimples could not be resolved in some areas by either SEM or TEM techniques (Fig. 45). There were undoubtedly dimples which could not be resolved since the above changes in microstructure should change only the scale of the fracture process and not change the fracture mode. Clearly, some fracture surfaces must be closely examined at high magnifications by TEM to determine if fracture has occurred by a localised microvoid-coalescence process and, even if dimples cannot be detected, such a process cannot be discounted. Small dimples on fracture surfaces produced in aggressive environments may

also be subsequently obscured by corrosion or film formation after fracture. Thus, one **cannot** conclude, as some workers have done, that fracture has occurred by decohesion on the basis that fracture surfaces appear to be flat when examined at high magnifications.

### 5.3 Dislocation Activity During Ductile and 'Brittle' Crack Growth

The occurrence of a more localised plastic-flow/microvoid-coalescence process when adsorbed metal or hydrogen atoms are present at crack tips must be due to an effect of adsorption on dislocation activity. The range of influence of adsorption is only several atomic distances for metals and, hence, adsorption can only affect the **nucleation** of dislocations at crack tips and the movement of screw dislocations intersecting crack tips. Such a localised effect can, nevertheless, explain all the experimental observations, as discussed below.

#### 5.3.1 Ductile Crack Growth

Ductile behaviour in inert environments can be explained on the basis that numerous dislocation sources **ahead** of crack tips are activated at lower stresses than that required for dislocation nucleation at crack tips. Only a few dislocations nucleated at sources **ahead** of crack tips egress **exactly** at crack tips to produce an increment of crack advance (and opening) — most either egress behind the crack tip producing only crack opening or just contribute to the **general strain** ahead of cracks (Fig. 46). Thus, crack-opening displacements are accommodated largely by blunting at crack tips and by the development of large strains ahead of cracks. The latter results in the nucleation and growth of voids at second-phase particles ahead of cracks, and macroscopic crack growth occurs by coalescence of blunt cracks with blunt voids.

The strains required for nucleation of voids (by fracture of particles or separation of particle/matrix interfaces) depend on the size, shape, and type of particle and, other things being equal, voids nucleate at lower strains around larger particles. In many materials, there are widely spaced large particles with smaller particles between them, and voids form preferentially around large particles some distance ahead of

cracks. Coalescence of these large voids with crack tips then involves formation of smaller voids around smaller particles so that small dimples between and within large, deep dimples are produced on fracture surfaces (Fig. 47). Egress of dislocations at and behind crack tips generally occurs in rather a chaotic fashion so that fracture surfaces are not usually macroscopically parallel to a low-index crystallographic plane.

### 5.3.2 Brittle Crack Growth

The occurrence of a more localised microvoid-coalescence process in liquid-metal, hydrogen, and aqueous environments than in inert environments can be explained on the basis that adsorption weakens interatomic bonds at crack tips, thereby facilitating the nucleation of dislocations from crack tips so that crack-tip sources are now activated before **extensive** dislocation activity occurs ahead of cracks. Dislocations injected from crack tips on suitably inclined slip planes produce crack advance (and opening) and, hence, crack-opening displacements are accommodated mainly by crack growth (Fig. 48a,b). Dislocation nucleation from crack tips often occurs in roughly equal amounts on slip planes on either side of cracks because any imbalance would produce a larger back-stress from dislocations previously injected on the more active slip plane, thereby promoting subsequent dislocation nucleation on the other slip plane.

This alternate-slip process is accompanied by sufficient dislocation activity ahead of cracks that some blunting occurs at crack tips and voids form just ahead of cracks. The coalescence of cracks growing by alternate-slip with voids just ahead of cracks essentially re-sharpens crack tips so that macroscopically brittle (transcrystalline) fractures are produced along a low-index crystallographic plane bisecting the two active slip planes (Fig. 48c). Crack fronts parallel to the line of intersection of the crack plane with the slip planes, i.e.  $\langle 110 \rangle$  directions in f.c.c. and b.c.c. metals, are also produced by such a process. If crack growth occurs in two  $\langle 110 \rangle$  directions, steps parallel to these directions form herringbone patterns (Fig. 49), as discussed in detail elsewhere [69].

Smaller strains and smaller plastic zones will obviously be developed when crack growth rather than crack blunting predominates. Thus, large second-phase particles some distance ahead of cracks are not enveloped by the plastic zone until they are close to the crack tip. Preferential void growth around the larger particles does not therefore occur to the same extent as occurs during ductile crack growth and, hence, predominantly small, shallow dimples are produced on 'brittle' fracture surfaces (Fig. 50). Voids can be nucleated by particles as small as  $\sim 5\text{nm}$  and there may well be sufficient very small particles to nucleate a high density of voids even in high-purity materials [70]. In the absence of particles, voids are probably nucleated at dislocation-cell boundaries and slip-band intersections [67, 68].

The proportion of dislocations injected from crack tips relative to those activated from near-crack-tip sources, i.e. the degree of embrittlement, will depend on the **adsorbed species** since different species will reduce the strength of interatomic bonds and thereby facilitate dislocation nucleation to different extents. The electronic interactions between adsorbate and substrate responsible for weakening of interatomic bonds are not well understood, although it is known that there are different kinds of adsorption, e.g. weak chemisorption, strong chemisorption [71]. Probably only weak chemisorption, which weakens interatomic bonds between substrate atoms without forming strong directional bonds between adsorbate and substrate atoms, facilitates dislocation nucleation.

Dislocation nucleation from crack tips should occur to a greater extent when the **surface coverage** of embrittling adsorbed atoms is larger since longer surface dislocation sources which require lower activation stresses should then operate. The effects of hydrogen pressure, temperature, and strain rate on the degree of embrittlement are probably associated with changes in surface coverage. The propensity for intercrystalline environmentally assisted cracking is probably due to preferential adsorption along the line of intersection of grain boundaries with surfaces (crack tips).

The degree of embrittlement should also be affected by the **microstructure** since this will determine, for example, the number and ease of operation of dislocation sources ahead of crack tips. Obstacles to dislocations such as precipitates probably inhibit extensive dislocation activity ahead of cracks more than dislocation injection from crack tips so that the degree of embrittlement is greater in higher strength materials. The alternate-slip/microvoid-coalescence process requires smaller strains in higher-strength materials probably also because there is a higher density of void nuclei and, consequently, less distance between crack tips and voids in higher-strength materials.

The above explanation for ductile versus brittle fracture is radically different from criteria [72,73] which are based on the relative stresses required for decohesion at crack tips and for slip on planes intersecting crack tips. Such criteria ignore the likelihood of dislocation activity ahead of cracks and predict that brittle fracture (decohesion) will occur when dislocation injection from crack-tips is difficult and, conversely, that ductile behaviour will occur when dislocation injection from crack tips occurs readily. The fracture energy will, of course, be greater if dislocation injection from crack tips occurs in preference to decohesion, but whether fracture is ductile or brittle on a macroscopic scale depends on the **distribution** of slip around cracks, as discussed above.

#### **5.4 Other Evidence for a Localised-Slip/Adsorption Mechanism**

##### **5.4.1 In-situ High-Voltage TEM Fracture Studies [74-79]**

Direct observations of dislocation activity during fracture of a number of materials (e.g. Ni, Fe, Al, Ti alloys) have shown that HAC in thin foils occurs by plastic flow, not by decohesion. Crack growth in a high-fugacity, atomic-hydrogen environment and in vacuum occurred by the injection of dislocations from crack tips, and sometimes involved the formation of small holes nucleated at dislocation-cell boundaries or slip-band intersections just ahead of cracks. However, crack growth occurred at lower stresses, and deformation around cracks was more localised, in hydrogen than in vacuum. Thus, the introduction of hydrogen around

stressed foils, containing stable cracks and stable dislocation structures ahead of cracks, resulted in crack growth involving dislocation injection from crack tips and intense dislocation activity ahead of cracks. Fracture occurred predominantly by a mode-III shearing displacement and involved considerable lateral contraction (thinning) of specimens ahead of crack tips. Dislocation activity was also increased in stressed, **uncracked** foils when hydrogen was introduced.

It was suggested that the effects of hydrogen on the fracture and deformation of thin foils were caused by **solute** hydrogen facilitating dislocation activity. Various explanations have been proposed [57,74,80] for this solid-solution softening but none of them has been definitely established. For example, segregation of hydrogen to dislocations could reduce the Peierls-Nabarro stress, enhance the rate of double-kink formation on screw dislocations, reduce the effectiveness of solutes (such as carbon) as dislocation pinning points, or produce a chemical driving force for dislocation motion.

Facilitating dislocation activity ahead of cracks could promote fracture in foils by facilitating the thinning process which occurs ahead of cracks. In bulk specimens, on the other hand, where fracture occurs predominantly by a mode-I opening displacement, facilitating dislocation activity ahead of cracks would probably not significantly increase the proportion of dislocations producing crack growth relative to those producing blunting, i.e. would not produce embrittlement. Furthermore, decreases in flow stress in bulk specimens due to the presence of solute hydrogen are observed only under certain conditions, whereas HAC occurs under a wide variety of conditions including those where serrated yielding and hardening are produced by solute hydrogen. Thus, the effects of **solute** hydrogen on dislocation activity are probably not significant during HAC in bulk specimens.

Adsorption-assisted dislocation injection from crack tips, proposed for HAC in bulk specimens, could also account for HAC in thin foils. Hydrogen adsorption on foil surfaces (and hydrogen-induced reductions of oxide films) could also facilitate the movement of dislocations intersecting foil surfaces for both cracked and uncracked specimens. Most

probably, both adsorbed hydrogen and solute hydrogen are responsible for HAC in thin foils, whereas HAC in bulk specimens is entirely due to adsorbed hydrogen.

#### 5.4.2 Surface Science Observations and Theoretical Considerations

It was suggested some time ago [81] that dislocation nucleation at surfaces could be inhibited if lattice spacings in the surface layers were different from bulk spacings. Recent low-energy-electron-diffraction (LEED) studies [82, 83] have shown that the spacing of atoms for several atomic layers just beneath **clean** surfaces is often significantly different from bulk values, i.e. 'relaxation' of the lattice occurs. Occasionally, the surface lattice even has a different lattice structure from the bulk, i.e. 'reconstruction' occurs. Relaxation occurs both normal to and parallel to the surface and is generally greater for more 'loosely-packed' atomic planes where relaxation of the lattice as deep as the **fifth** atomic layer has been reported. The spacing of atoms between the first and second layers is generally contracted (by up to ~22%) compared with the bulk but subsequent layers may be either contracted or expanded depending on the material and surface crystallography [84]. Surface relaxations and reconstructions essentially occur because surface atoms have fewer neighbours than those in the bulk, and it is therefore not surprising that adsorption of **some** species, by effectively increasing the number of neighbours around surface atoms, often removes the surface relaxation or reconstruction. However, adsorption may sometimes produce an expansion of the surface lattice or induce a reconstruction [82, 85]. Environmental species such as oxygen which form strongly bonded compounds with the base metal are generally incorporated into the topmost or sub-surface layers of metal atoms, producing an incipient film.

Computer simulations of crack growth [86, 87] have suggested that dislocation nucleation should be inhibited when the lattice parameter of several atomic layers around the crack tip is smaller than the bulk, and should be enhanced when the lattice parameter is large, than the bulk, as a result of surface stresses induced by the mismatch in lattice parameters. Thus, clean-surface relaxations at tips of cracks growing in vacuum or inert gases, and incipient oxide films at tips of cracks growing

in air, could well be responsible for inhibiting dislocation nucleation from crack tips so that crack growth occurs by egress of dislocations from near-crack-tip sources, producing ductile behaviour. (The egress of dislocations at surfaces is probably less affected by surface relaxations than dislocation injection from surfaces since the former will be promoted by an attractive image force and the kinetic energy of dislocations.) Conversely, the removal of surface relaxations due to adsorption could well facilitate dislocation nucleation from surfaces so that crack growth occurs predominantly by dislocation injection from crack tips, producing 'brittle' behaviour. Other theoretical analyses also suggest that dislocation nucleation from crack tips could be affected by adsorption-induced changes in the surface stress [88].

Atomistic calculations of crack growth in nickel using an 'embedded-atom method' [89, 90] indicate that adsorbed hydrogen can weaken interatomic bonds so that decohesion or dislocation nucleation at crack tips occurs at a lower stress than that required in inert environments. Quantum-mechanical cluster calculations for adsorbed hydrogen on beryllium [91] suggest that high tensile stresses could be induced in the surface layers by adsorption thereby facilitating dislocation nucleation. Cluster calculations have also shown that the presence of impurity atoms can decrease the electron density between metal atoms thereby possibly reducing their interatomic bond strength [92, 93].

Experimental confirmation that adsorption facilitates nucleation of dislocations using **uncracked** specimens is difficult to obtain since adsorption cannot easily be isolated from other processes. For example, the stress-strain behaviour of specimens with large surface-to-volume ratios should be affected by adsorption but removal of oxide films to enable adsorption to occur, or diffusion of environmental atoms into specimens prior to testing, would themselves influence stress-strain behaviour. Field-ion-microscopy observations of iron surfaces in the presence of hydrogen did suggest that adsorbed hydrogen facilitated dislocation nucleation [94], but other effects may possibly have been involved.

Data for the effects of hydrogen pressure, temperature, and other variables on the kinetics of HAC/SCC have not generally helped determine the **mechanisms** of cracking. However, analysis of such data along with surface-science studies in steels suggest that adsorption of hydrogen atoms (involving adsorbed molecular hydrogen precursor states) is the rate-controlling step for HAC, and that there is a correlation between the degree of embrittlement and the surface coverage of adsorbed hydrogen in some circumstances [95-97]. On the other hand, there are undoubtedly circumstances where hydrogen diffusion to internal cracks controls the cracking kinetics [98].

The considerations above generally support an adsorption-induced localised-slip process for environmentally assisted cracking. However, it should be noted that the surface-science observations were generally made using annealed specimens with atomically flat surfaces parallel to low-index crystallographic planes. The situation at the tips of growing cracks, where crack-tip surfaces are stepped (due to emergent dislocations) and not parallel to a low-index plane, is probably significantly different. The theoretical models also necessarily contain many simplifying features and their relevance to real crack tips is not known. Nevertheless, further work such as atomistic calculations of the effects of embrittling and non-embrittling metal atoms (see Appendix I) on interatomic bonding could provide further insights into the processes occurring on the electronic scale during environmentally assisted cracking.

## 6. CONCLUDING REMARKS

The results reported in the present overview have largely been concerned with crack growth under sustained or monotonically increasing loads but similar results have also been obtained for crack growth under cyclic loading for many of the materials and environments considered [99, 100]. For example, fatigue crack growth of nickel single crystals in liquid mercury and gaseous hydrogen environments also produces {100} <110> fracture surfaces with extensive slip on {111} planes intersecting cracks; the spacing of 'brittle' striations on fracture surfaces produced in mercury and hydrogen environments was the same and approximately three

times the spacing of 'ductile' striations produced in inert environments (Figs 51,52). Such effects can also be explained on the basis that adsorption facilitates dislocation injection from crack tips so that crack growth occurs by an alternate-slip process. For fatigue, deformation behind the crack tip during unloading resharpens the crack tip and thereby produces striations [99, 100]. The formation of voids ahead of cracks (which resharpens cracks growing by alternate-slip under sustained or monotonically increasing stresses) is therefore not essential during fatigue.

An adsorption-induced localised-slip process for environmentally assisted cracking could also be applicable to some materials not mentioned in the present overview. For example, such a mechanism could account for SCC of (fcc) stainless steels where cleavage-like {100} <110> fracture surfaces, with significant slip on {111} planes intersecting cracks, are sometimes produced [101,102]. Intercrystalline HAC of austenitic stainless steels (with hydrogen diffusivities  $\sim 10^{-11}$ - $10^{-12}$  cm<sup>2</sup>/s) in high-pressure hydrogen can also occur at sufficiently high velocities ( $\sim 10^{-3}$  cm/s) that probably only adsorbed hydrogen, and hydrogen in the first few atomic layers beneath crack tips, are present [103]. An adsorption-induced localised-slip process has also been proposed for HAC and LME in Fe- and Ni- based amorphous alloys [104,105].

Finally, it should be emphasised that there are many systems where adsorption is **not** responsible for HAC and SCC. For example, it is well established that HAC in hydride-forming materials can occur by formation and subsequent cleavage of brittle hydrides ahead of cracks [106], and that intercrystalline SCC occurs predominantly by localised dissolution in some materials and environments [107]. The formation of brittle films at crack tips may also result in SCC in some circumstances [108]. Combinations of processes or different processes at different stress-intensity factors (crack velocities) for the same material and environment may well occur in some cases. Nevertheless, the observations reviewed in this report show that an adsorption-induced localised-slip process is one of the more common processes responsible for environmentally assisted cracking.

**ACKNOWLEDGEMENTS**

The author would like to thank Phil Trevena, AERE, Harwell, U.K. for assistance with testing specimens in liquid alkali metals. Thanks are also due to Horst Vehoff, Max-Planck-Institut für Eisenforschung, FRG, for the gift of the Fe-Si single crystals.

**REFERENCES**

1. The Theory of Stress Corrosion Cracking in Alloys [Editor: J.C. Scully], NATO, Brussels, 1971.
2. Effect of Hydrogen on Behavior of Materials [Editors: A.W. Thompson and I.M. Bernstein], A.I.M.E., New York, 1976.
3. Stress Corrosion Cracking and Hydrogen Embrittlement of Iron Base Alloys [Editors: R.W. Staehle, J. Hochmann, R.D. McCright and J.E. Slater], NACE - 5, Houston, Tx, 1977.
4. Hydrogen in Metals Proc. 2nd International Congress, Paris 1977, Pergamon Press, Oxford, 1977.
5. Hydrogen Effects in Metals [Editors: I.M. Bernstein and A.W. Thompson], Metall. Soc. A.I.M.E., Warrendale, Pa, 1981.
6. Atomistics of Fracture [Editors: R.M. Latanision and J.R. Pickens], Plenum Press, New York, 1983.
7. Embrittlement by Liquid and Solid Metals [Editor: M.H. Kamdar], Metall. Soc. A.I.M.E., Warrendale, Pa, 1984.
8. Hydrogen Degradation of Ferrous Alloys [Editors: R.A. Oriani, J.P. Hirth, M. Smialowski], Noyes Publ., Park Ridge, N.J., 1985.

9. J.A. Feeney and M.J. Blackburn, The Status of Stress Corrosion Cracking of Titanium Alloys in Aqueous Solutions, in ref. 1, pp. 355-397.
10. M.O. Speidel, Current Understanding of Stress Corrosion Crack Growth in Aluminum Alloys, in ref. 1, pp. 289-354.
11. N.S. Stoloff and T.L. Johnston, Crack Propagation in a Liquid Metal Environment, Acta Metall., Vol. 11, 1963, pp. 251-256.
12. A.R.C. Westwood, C.M. Preece, and M.H. Kamdar, Application of a Crack Propagation Criterion to Liquid-Metal Embrittlement; Cleavage of Aluminium Monocrystals in Liquid Gallium, Trans. ASM, Vol. 60, 1967, pp. 723-725.
13. M.H. Kamdar, Embrittlement by Liquid Metals, Prog. Mater. Sci., Vol. 15, 1973, pp. 289-374.
14. N.S. Stoloff, Liquid and Solid Metal Embrittlement, in ref. 6, pp. 921-949.
15. C.F. Old, Micromechanisms of Crack Growth in Liquid Metal Environments, Metal Sci., Vol. 14, 1980, pp. 433-440.
16. F.A. Shunk and W.R. Warke, Specificity as an Aspect of Liquid-Metal Embrittlement, Scripta Metall., Vol. 8, 1974, pp. 519-526.
17. A.R.C. Westwood and M.H. Kamdar, Concerning Liquid Metal Embrittlement, particularly of Zinc Monocrystals by Mercury, Phil. Mag., Vol. 8, 1963, pp. 787-804.
18. S.P. Lynch, Mechanisms of Fracture in Liquid-Metal Environments, in ref. 7, pp. 105-115.

19. S.P. Lynch, Effect of Environment on Fracture — Mechanisms of Liquid-Metal Embrittlement, Stress-Corrosion Cracking and Corrosion Fatigue, Fracture 1977, Vol. 2 [Editor: D.M.R. Taplin], University of Waterloo Press, 1977, pp. 859-866.
20. S.P. Lynch, "Cleavage" of Aluminium Single Crystals in Liquid-Metal Environments, Mater. Sci. Engng, Vol. 72, 1985, pp. L33-L37.
21. S.P. Lynch, Liquid-Metal Embrittlement in an Al16%Zn3%Mg Alloy, Acta Metall., Vol. 29, 1981, pp. 325-340.
22. W.H. Johnson, On Some Remarkable Changes Produced in Iron and Steel by the Action of Hydrogen and Acids, Royal Society of London Proceedings, Vol. 23, 1874-75, pp. 168-180: Republished in Hydrogen Damage [Editor: C.D. Beachem], ASM, Metals Park, Ohio, 1977, pp.1-11.
23. H. Nichols and W. Rostoker, Analogies Between Stress-Corrosion Cracking and Embrittlement by Liquid Metals, Trans. ASM, Vol. 56, 1963, pp. 494-507.
24. A.S. Tetelman and S. Kunz, A Unified Model for Hydrogen Embrittlement, Liquid Metal Embrittlement, and Temper Embrittlement due to Weakening of Atomic Bonds, in ref. 3, pp. 359-375.
25. A.W. Funkenbusch, L.A. Heldt, and D.F. Stein, The Influence of Grain Boundary Phosphorus Concentration on Liquid Metal and Hydrogen Embrittlement of Monel 400, Metall. Trans. A, Vol. 13, 1982, pp. 611-618.
26. C.E. Price and R.S. Fredell, A Comparative Study of the Embrittlement of Monel 400 at Room Temperature by Hydrogen and Mercury, Metall. Trans. A, Vol. 17, 1986, pp. 889-898.

27. S.P. Lynch and N.E. Ryan, Mechanisms of Hydrogen Embrittlement - Crack Growth in a Low-Alloy Ultra-High-Strength Steel under Cyclic and Sustained Stresses in Gaseous Hydrogen, in ref. 4, Paper 3D12.
28. S.P. Lynch, A Comparative Study of Stress-Corrosion Cracking, Hydrogen-Assisted Cracking and Liquid-Metal Embrittlement in Al, Ni, Ti and Fe-Based Alloys, in ref. 5, pp. 863-870.
29. S.P. Lynch, Mechanisms of Environmentally Assisted Cracking in Al-Zn-Mg Single Crystals, Corros. Sci., Vol. 24, 1984, pp. 925-937.
30. S.P. Lynch, Further Observations of Environmentally Assisted Cracking in Al-Zn-Mg Single Crystals, Corros. Sci., Vol. 24, 1984, pp. 375-378.
31. S.P. Lynch, Mechanisms of Stress-Corrosion Cracking and Liquid-Metal Embrittlement in Al-Zn-Mg Bicrystals, J. Mater. Sci., Vol. 20, 1985, pp. 3329-3338.
32. S.P. Lynch, A. Fractographic Study of Hydrogen Assisted Cracking and Liquid-Metal Embrittlement in Nickel, J. Mater. Sci., Vol. 21, 1986, pp. 692-704.
33. S.P. Lynch and P. Trevena, Stress-Corrosion Cracking and Liquid-Metal Embrittlement in Pure Magnesium, submitted to Corrosion, 1986.
34. S.P. Lynch, Environmentally Assisted Cracking at High Velocities, Scripta Metall., to be published, Feb 1987.
35. S.P. Lynch, Unpublished work.

36. S.P. Lynch, A. Fractographic Study of Gaseous Hydrogen Embrittlement and Liquid-Metal Embrittlement in a Tempered-Martensitic Steel, *Acta Metall.*, Vol. 32, 1984, pp. 79-90.
37. C. D. Beachem, Microscopic Fracture Processes, Fracture, Vol. 1, Microscopic and Macroscopic Fundamentals, [Editor: H. Liebowitz], Academic Press, New York, 1968, pp. 243-349.
38. D. Broek. A Critical Note on Electron Fractography, *Engng. Frac. Mech.*, Vol. 1, 1970, pp. 691-695.
39. H. Vehoff and W. Rothe, Gaseous Hydrogen Embrittlement in FeSi- and Ni- Single Crystals, *Acta Metall.*, Overview No. 30, Vol. 31, 1983, pp. 1781 - 1793.
40. I. Aitchison and B. Cox, Interpretation of Fractographs of SCC in Hexagonal Metals, *Corrosion*, Vol. 28, 1972, pp. 83-87.
41. R.H. Van Stone, J.R. Low Jr., and J.L. Shannon Jr., Investigation of the Fracture Mechanism of Ti-5Al-2.5Sn at Cryogenic Temperatures, *Metall. Trans. A*, Vol. 9, 1978, pp. 539-552.
42. D.A. Meyn and G. Sandoz, Fractography and Crystallography of Subcritical Crack Propagation in High Strength Titanium Alloys, *Trans. Met. Soc. AIME*, Vol. 245, 1969, pp. 1253-1258.
43. H.H. Johnson, Hydrogen Gas Embrittlement, Hydrogen in Metals, [Editor: I.M. Bernstein and A.W. Thompson], ASM, Metals Park, Ohio, 1974, pp. 35-49.
44. P. McIntyre, The Relationships between Stress Corrosion Cracking and Sub-Critical Flaw Growth in Hydrogen and Hydrogen Sulphide Gases, in ref. 3, pp. 788-796.

45. J. Renner and H.J. Grabke, Determination of Diffusion Coefficients in the Hydriding of Alloys, *Z. Metallk.*, Vol. 69, 1978, pp. 639-642.
46. T. Ishikawa and R.B. McLellan, The Diffusivity of Hydrogen in Aluminium, *Acta Metall.*, Vol. 34, 1986, pp. 1091-1095.
47. C.D.S. Tuck and G.M. Scamans, Comparative Hydrogen Permeation Studies of Aluminium Alloys Exposed to Water Vapour, in ref. 4, Paper 4A11.
48. K. Kiuchi and R.B. McLellan, The Solubility and Diffusivity of Hydrogen in Well-Annealed and Deformed Iron, *Acta Metall.*, Vol. 31, 1983, pp. 961 - 984.
49. L. -y Lin, X. -y Huang, Y. -k Li, and C. -m Hsiao, A New Mechano-Electrochemical Method for the Determination of the Diffusion Coefficient of Hydrogen in Valve Metals, *Scripta Metall.*, Vol. 16, 1982, pp. 1387-1391.
50. J.L. Walsman, G. Sines, and R.F. Toosky, Measurement of the Diffusivity of Hydrogen in Titanium at Room Temperature, in ref. 4, Paper 1011.
51. I.I. Philips, P. Poole, and L.L. Shreir, Hydride Formation During Cathodic Polarization of Ti, *Corros. Sci.*, Vol. 12, 1972, pp. 855-866.
52. E. Brauer, R. Gruner, and F. Rauch, Hydrogen Diffusivity in Titanium Single Crystals, *Ber. Bunsenges. Phys. Chemie.*, Vol. 87, 1983, pp. 341-345.
53. W.M. Robertson, Hydrogen Permeation, Diffusion and Solution in Nickel, *Z. Metallk.*, Vol. 64, 1973, pp. 436-443.

54. K.A. Lee and R.B. McLellan, The Diffusivity of Hydrogen in Nickel at Low Temperatures, Scripta Metall., Vol. 18, 1984, pp. 859-861.
55. J.K. Tien, S.V. Nair, and R.R. Jensen, Dislocation Sweeping of Hydrogen and Hydrogen Embrittlement, in ref. 5, pp. 37-53.
56. J. Albrecht, I.M. Bernstein, and A.W. Thompson, Evidence for Dislocation Transport of Hydrogen in Aluminium, Metall. Trans. A, Vol. 13, 1982, pp. 811-820.
57. J.P. Hirth, Effects of Hydrogen on the Properties of Iron and Steel, Metall. Trans. A, Vol. 11, 1980, pp. 861-890.
58. W. Wei, Crack Kinetics in the Nickel-Hydrogen System, Ph. D. Thesis, University of Illinois, 1984.
59. T. Tsuru and R.M. Latanision, Grain Boundary Transport of Hydrogen in Nickel, Scripta Metall., Vol. 16, 1982, pp. 575-578.
60. J. Du Plessis, E. Andrieu, and J.P. Henon, The Effect of Stress on Hydrogen Permeation in Nickel, Scripta Metall., Vol. 20, 1986, pp. 163-166.
61. P. Studebaker, C. Altstetter, and W. Conley, Hydrogen Permeation of Stainless Steel Under Stress, in ref. 5, pp. 169-175.
62. M.I. Baskes, C.F. Melius, and W.D. Wilson, Hybrid Calculations of the Properties of Hydrogen in Metals, in ref. 5, pp. 67-74.
63. J. Eastman, F. Heubaum, T. Matsumoto, and H.K. Birnbaum, The Effect of Hydrogen on the Solid Solution Strengthening and Softening of Nickel, Acta Metall., Vol. 30, 1982, pp. 1579 - 1586.

64. A. Kimura and H. Kimura, Hydrogen Embrittlement in High Purity Iron Single Crystals, Mater. Sci. Engng., Vol. 77, 1986, pp. 75-83.
65. T.F. Klimowicz and R.M. Latanision, On the Embrittlement of Aluminium Alloys by Cathodic Hydrogen: The Role of Surface Films, Metall. Trans. A, Vol. 9, 1978, pp. 597-599.
66. C.D. Beachem, A New Model for Hydrogen Assisted Cracking (Hydrogen 'Embrittlement'), Metall. Trans., Vol. 3, 1972, pp. 437-451.
67. R.N. Gardner, T.C. Pollock, and H.G.F. Wilsdorf, Crack Initiation at Dislocation Cell Boundaries in the Ductile Fracture of Metals, Mater. Sci. Engng., Vol. 29, 1977, pp. 169-174.
68. H.G.F. Wilsdorf, Review Paper - The Ductile Fracture of Metals: A Microstructural Viewpoint, Mater. Sci. Engng., Vol. 59, 1983, pp. 1-39.
69. S.P. Lynch, Herringbone Patterns on Fracture Surfaces, Scripta Metall., Vol. 20, 1986, pp. 1067-1072.
70. A.W. Thompson and P.F. Weihrach, Ductile Fracture: Nucleation at Inclusions, Scripta Metall., Vol. 10, 1976, pp. 205-210.
71. T.E. Fischer, Surface Effects in Crystal Plasticity: Overview from a Surface Science Point of View, Surface Effects in Crystal Plasticity, [Editor: R.M. Latanision and J.T. Fourie], Noordhoff, Leyden, The Netherlands, 1977, pp. 127-160.
72. A. Kelly, W.R. Tyson, and A.H. Cottrell, Ductile and Brittle Crystals, Phil. Mag., Vol. 15, 1967, pp. 567-586.

73. J.R. Rice and R. Thomson, Ductile versus Brittle Behaviour of Crystals, *Phil. Mag.*, Vol. 29, 1974, pp. 73-96.
74. T. Matsumoto, J. Eastman, and H.K. Birnbaum, Direct Observations of Enhanced Dislocation Mobility due to Hydrogen, *Scripta Metall.*, Vol. 15, 1981, pp. 1033-1037.
75. T. Tabata and H.K. Birnbaum, Direct Observations of Hydrogen Enhanced Crack Propagation in Iron, *Scripta Metall.*, Vol. 18, 1984, pp. 231-236.
76. I.M. Robertson and H.K. Birnbaum, An HVEM Study of Hydrogen Effects on the Deformation and Fracture of Nickel, *Acta Metall.*, Vol. 34, 1986, pp. 353-366.
77. T. Tabata and H.K. Birnbaum, Direct Observations of the Effect of Hydrogen on the Behavior of Dislocations in Iron, *Scripta Metall.*, Vol. 17, 1983, pp. 947-950.
78. G.M. Bond, I.M. Robertson, and H.K. Birnbaum, On the Determination of the Hydrogen Fugacity in an Environmental Cell TEM Facility, *Scripta Metall.*, Vol. 20, 1986, pp. 653-658.
79. I.M. Robertson, Unpublished work, University of Illinois, 1985.
80. J.C.M. Li, C.G. Park, and S.M. Ohr, Chemical Driving Force for Dislocation Motion in Hydrogen Embrittlement, *Scripta Metall.*, Vol. 20, 1986, pp. 371-376.
81. R.L. Fleischer, Effects of Non-Uniformities on the Hardening of Crystals, *Acta Metall.*, Vol. 8, 1960, pp. 598-604.
82. G.A. Somorjai and M.A. van Hove, Structure and Bonding, Vol. 38 [Editors: J.D. Dunitz et al.], Springer, Berlin, 1979.

83. J. Sokolov, F. Jona, and P.M. Marcus, Multilayer Relaxation of the Fe {210} Surface, *Phys. Rev. B*, Vol. 31, 1985, pp. 1929-1935.
84. U. Landman, R.N. Barnett, C.L. Cleveland, and R.H. Rast, Theoretical Considerations of Energetics, Dynamics and Structure at Interfaces, *J. Vac. Sci. Technol. A*, Vol. 3, 1985, pp. 1574-1587.
85. P. Marcus and J. Oudar, Gas Surface Equilibria, in ref. 8, pp. 36-77.
86. A. Paskin, K. Sieradzki, D.K. Som, and G.J. Dienes, Dislocation Enhancement and Inhibition Induced by Films on Crack Surfaces, *Acta Metall.*, Vol. 31, 1983, pp. 1253-1265.
87. A. Paskin, B. Massoumzadeh, K. Sieradzki, and G.J. Dienes, Enhancement of Dislocation Generation Induced by Films on Crack Surfaces, *Scripta Metall.*, Vol. 18, 1984, pp. 1135-1138.
88. R. Thomson, T. -J. Chuang, and I. -H. Lin, The Role of Surface Stress in Fracture, *Acta Metall.*, Vol. 34, 1986, pp. 1133-1143.
89. M.S. Daw and M.I. Baskes, Embedded-Atom Method: Derivation and Application to Impurities, Surfaces and Other Defects in Metals, *Phys. Rev. B*, Vol. 29, 1984, pp. 6443-6453.
90. M.S. Daw and M.I. Baskes, unpublished work, Sandia National Laboratory, 1985.
91. B.N. Cox and C. W. Bauschlicher Jr., Surface Relaxation and Induced Stress Accompanying the Adsorption of H on Be (0001), *Surf. Sci.*, Vol. 102, 1981, pp. 295-311.

92. R.P. Messmer and C.L. Briant, A. Theoretical Approach to Embrittlement of Metals: The Quantum Mechanical Cluster Method, in ref. 8, pp. 140-166.
93. M.E. Eberhart, R.M. Latanision, and K.H. Johnson, The Chemistry of Fracture: A Basis for Analysis, Acta Metall., Vol. 33, 1985, pp. 1769-1783.
94. J.A. Clum, The Role of Hydrogen in Dislocation Generation in Iron Alloys, Scripta Metall., Vol. 9, 1975, pp. 51-58.
95. R.W. Pasco and P.J. Ficalora, Gaseous Hydrogen Embrittlement - The Rate Controlling Process, Scripta Metall., Vol. 15, 1981, pp. 1019-1022.
96. R.W. Pasco and P.J. Ficalora, A Work Function - Chemisorption Study of Hydrogen on Iron: Kinetic and Strain Effects, Acta Metall., Vol. 31, 1983, pp. 541-558.
97. R.H. Jones and D.R. Baer, Relationship Between Surface Hydrogen and Fracture Stress of 4340 Steel, Scripta Metall., Vol. 20, 1986, pp. 927-932.
98. R.P. Wei and M. Gao, Chemistry, Microstructure and Crack Growth Response, in ref. 8, pp. 579-607.
99. S.P. Lynch, Mechanisms of Fatigue and Environmentally Assisted Fatigue, Fatigue Mechanisms [Editor: J.T. Fong], ASTM STP 675, 1979, pp. 174-213.
100. S.P. Lynch, Mechanisms of Environmentally Assisted Fatigue in Nickel and Al-Zn-Mg Single Crystals, Fatigue 84 [Editor: C.J. Beevers], Chameleon Press, London, 1984, pp. 445-454.

101. J.M. Silcock, Orientations of Transgranular Stress Corrosion Cracks In Austenitic Steels Tested in  $MgCl_2$  Solutions, Br. Corros. J., Vol. 16, 1981, pp. 78-93.
102. R. Koterazawa and D. Shimo, Stress Corrosion Cracking of a SUS 304 Stainless Steel in  $MgCl_2$  Solution, Jap. Soc. Mater. Sci., Vol. 27, 1978, pp. 1158-1164 .
103. M.W. Perra and R.E. Stoltz, Sustained Load Cracking of a Precipitation-Strengthened Austenitic Steel in High-Pressure Hydrogen, in ref. 5, pp. 645-652.
104. S. Ashok, N.S. Stoloff, M.E. Glicksman, and T. Slavin, Liquid Metal and Hydrogen Embrittlement of Amorphous Alloys, Scripta Metall., Vol. 15, 1981, pp. 331-337.
105. T.P. Slavin and N.S. Stoloff, Environmental Cracking of Metallic Glasses, Mater. Sci. Engng., Vol. 68, 1984, pp. 55-71.
106. H.K. Birnbaum, Hydrogen Related Fracture of Metals, in ref. 6, pp. 733-765.
107. R.N. Parkins, Stress Corrosion Cracking, in ref. 6, pp. 969-990.
108. K. Sieradzki and R.C. Newman, Brittle Behaviour of Ductile Metals during Stress-Corrosion Cracking, Phil. Mag. A, Vol. 51, 1985, pp. 95-132.

APPENDIX I

Specificity of LME for **transcrystalline** (cleavage-like) cracking in notched specimens of various pure metals and alloys tested in pure liquid-metal environments at temperatures within 50°C of the melting-point\* of the liquid metal : E - LME observed, although the severity varies widely; N - not embrittled for conditions used [35].

Material	Liquid-Metal Environment								
	Hg *(-39)	Ga (-30)	In (-156)	Sn (-232)	Li (-179)	Na (-98)	K (-63)	Rb (-39)	Cs (-28)
Ni	E	N	N	N	E	E	N	N	N
Al	E	E	E	E					
Cu/ α-brass	N†	N†	N	N					
β-brass	E	E							
Fe-Si	E		E	E	E				
Mg	N	N				E	E	E	E
Ti	E	N							

†N.B. Intercrystalline LME occurs in these and possibly other systems listed as not embrittled. Attempts to understand the specificity of LME should be based on data for transcrystalline LME since intercrystalline LME may be complicated by the segregation of (often unknown) impurities at grain boundaries.

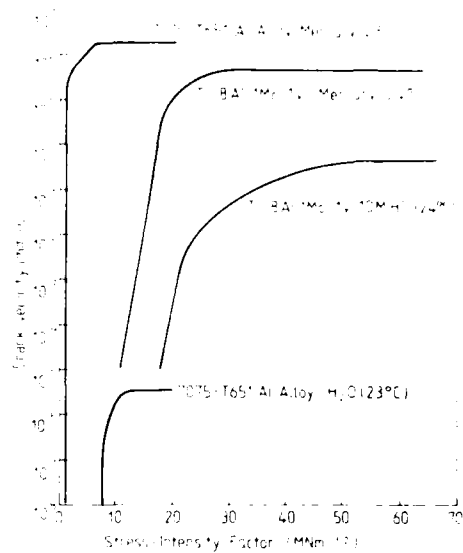


**Figure 1.** Graphs of crack velocity versus stress-intensity factor for aluminium and titanium alloys tested in liquid metal and aqueous environments. (Replotted from data in refs 9, 10).

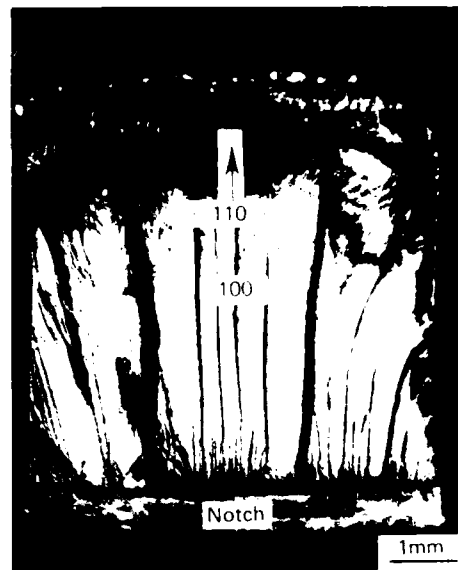


**Figure 2.** Optical micrograph of cleavage-like fracture surface of pure aluminium single crystal cracked in liquid gallium at  $-30^{\circ}\text{C}$ .

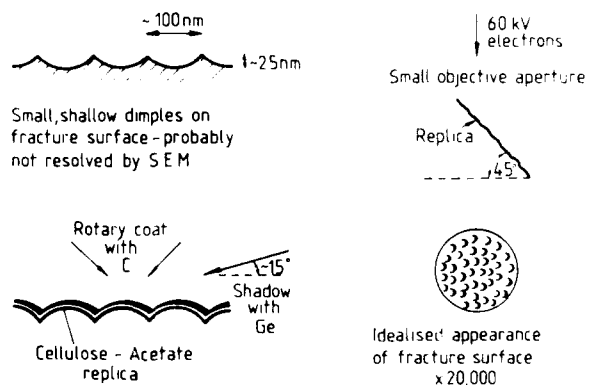


**Figure 3.** Schematic diagram illustrating the procedures used for the preparation and examination of secondary-carbon replicas of fracture surfaces by TEM. Smaller, shallower features can be detected by this technique than by SEM.

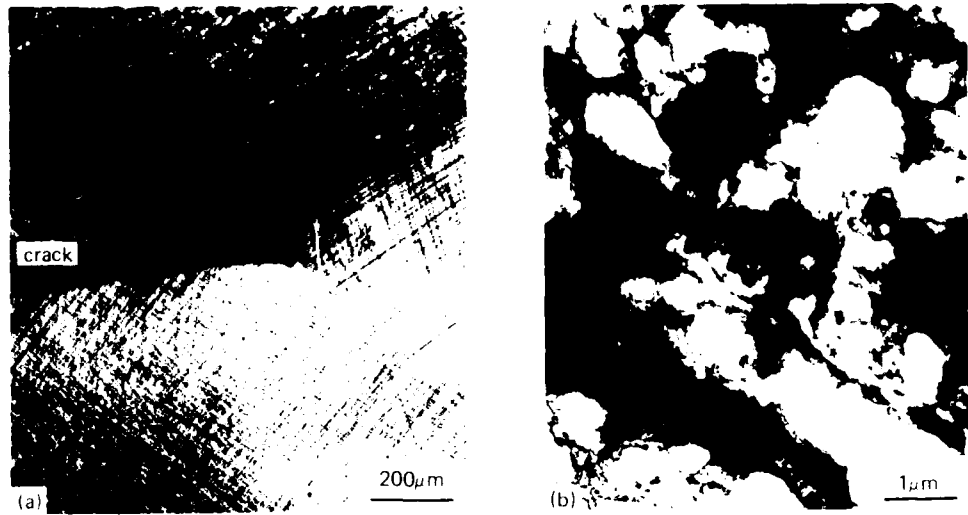


**Figure 4.** (a) Optical micrograph showing extensive slip around {100} cleavage-like crack (which is filled with the solidified eutectic), and (b) TEM micrograph of dislocation-cell structure just beneath fracture surface, in a pure (99.99%) aluminium single crystal cracked in a low-melting-point liquid Bi-Pb-In-Sn-Cd eutectic at  $-60^{\circ}\text{C}$ .

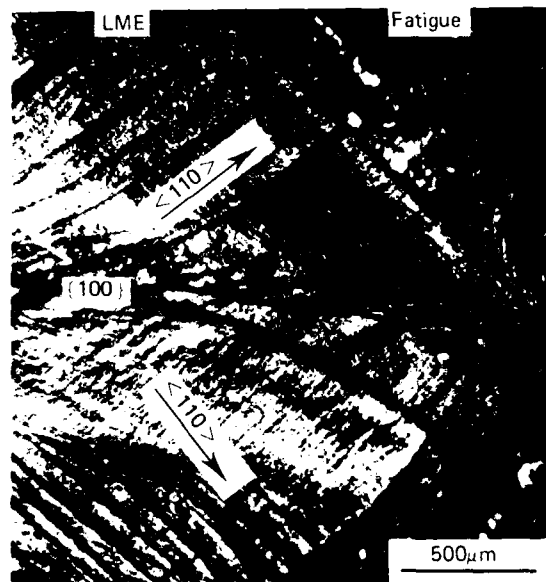


**Figure 5.** Optical micrograph of fracture surface produced in a pure aluminium single crystal by crack growth in the liquid eutectic at  $-60^{\circ}\text{C}$  and then by fatigue in air at  $20^{\circ}\text{C}$ . Crack growth in the liquid eutectic occurred on a {100} plane in two <110> directions so that the crack front was a V-shape. Closely spaced slip lines parallel to, and steps normal to, the crack front are evident.



**Figure 6.** TEM of fracture surface for a pure aluminium single crystal cracked in the liquid-alloy environment at  $-60^{\circ}\text{C}$ , showing small dimples and an orthogonal network of slip lines.

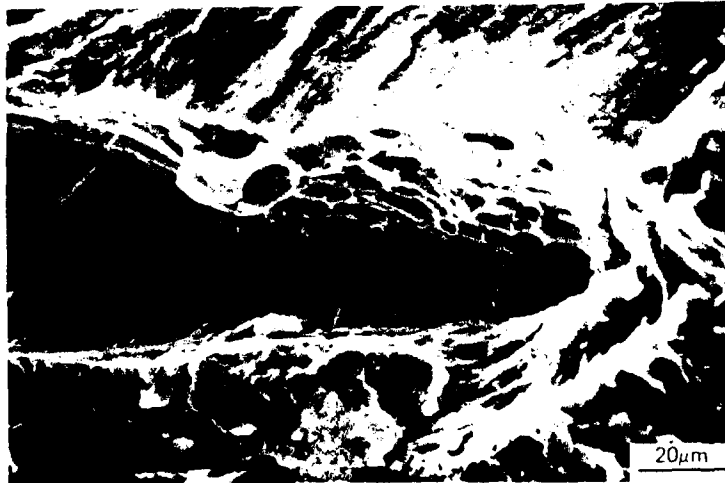


**Figure 7.** SEM of secondary  $\{100\}$  crack, normal to the primary fracture surface, in a pure aluminium single crystal cracked in the liquid-alloy environment at  $-60^{\circ}\text{C}$ , showing dimples on the crack walls.

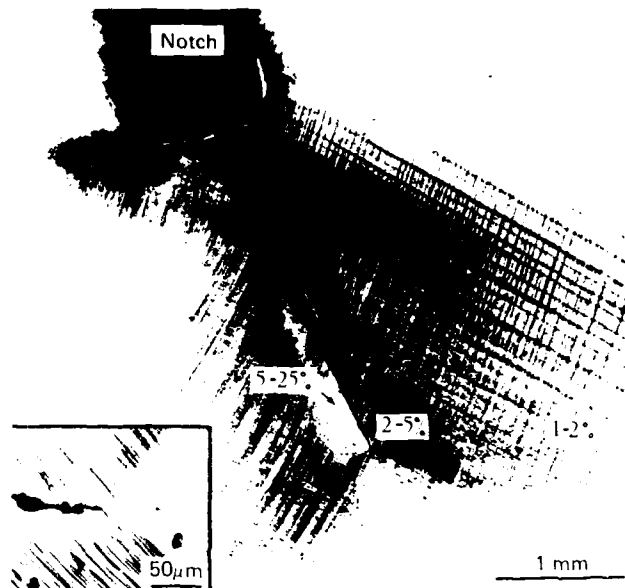


**Figure 8.** Optical micrograph of polished and etched section showing slip pattern around a {100} cleavage-like crack in the interior of a solution-treated Al-Zn-Mg alloy (HV-70) cracked in the liquid-alloy environment at  $-60^{\circ}\text{C}$ . Estimated strains (determined by comparing the etched appearance with that in specimens given known strains) are indicated. An optical micrograph of the slip pattern on the specimen side surface for the same crack is shown in the inset.

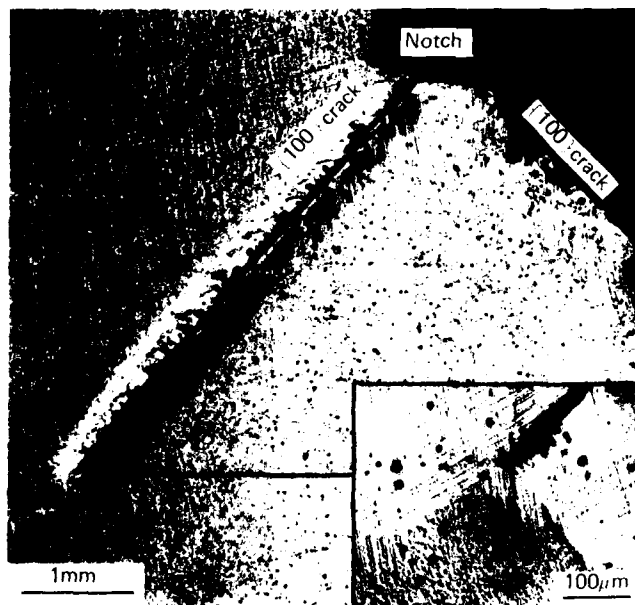


**Figure 9.** Optical micrographs of polished and etched section showing slip pattern around a {100} cleavage-like crack in the interior of a peak-aged Al-Zn-Mg alloy (HV-160) cracked in the liquid-alloy environment at  $-60^{\circ}\text{C}$ .

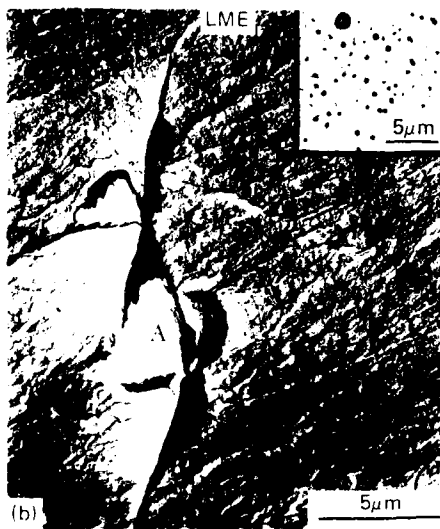
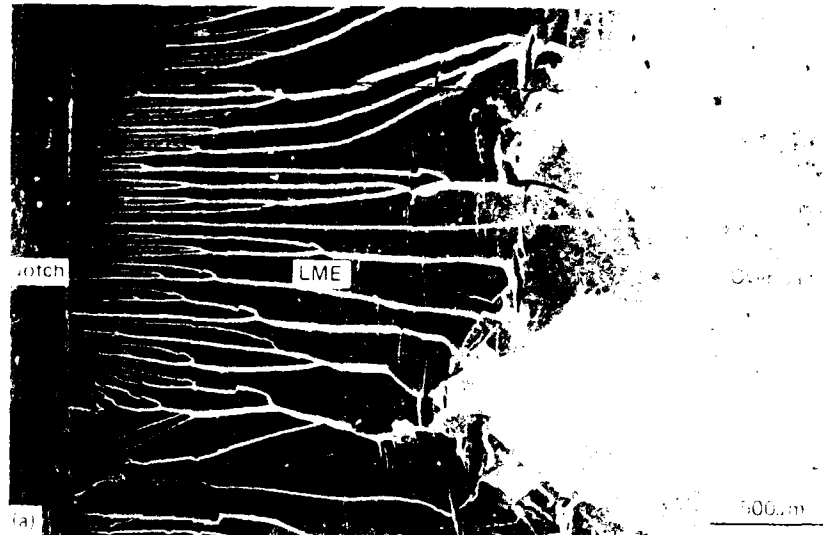


**Figure 10.** (a) SEM of fracture surface produced by crack growth in liquid gallium (at  $-30^{\circ}\text{C}$ ) and then in air (when the limited supply of gallium was exhausted) in a grossly overaged Al-Zn-Mg single crystal (HV-70), showing river lines and secondary cracks on the cleavage-like fracture surface produced in gallium, and large dimples on the ductile fracture surface produced in air, (b) TEM of replica of cleavage-like area showing small, shallow dimples and an isolated large dimple, A, which had nucleated a secondary crack, and (c) TEM of replica of ductile area showing small, stretched dimples within the large, deep dimples. Inset is an optical micrograph of the precipitate distribution.



**Figure 11.** SEM and TEM of fracture surface produced in an overaged Al-Zn-Mg single crystal (HV-100) by rapid crack growth ( $\sim 10$  mm/s) in distilled water at  $20^\circ\text{C}$ , showing (a) macroscopic, cleavage-like appearance, and (b-d) microscopic appearance: Y-shaped tear ridges associated with large dimples, a cracked inclusion (A) within a large dimple, and very small dimples and closely spaced slip lines between the ridges are evident. Inset is a TEM of a thin foil showing the dispersion of ageing precipitates.

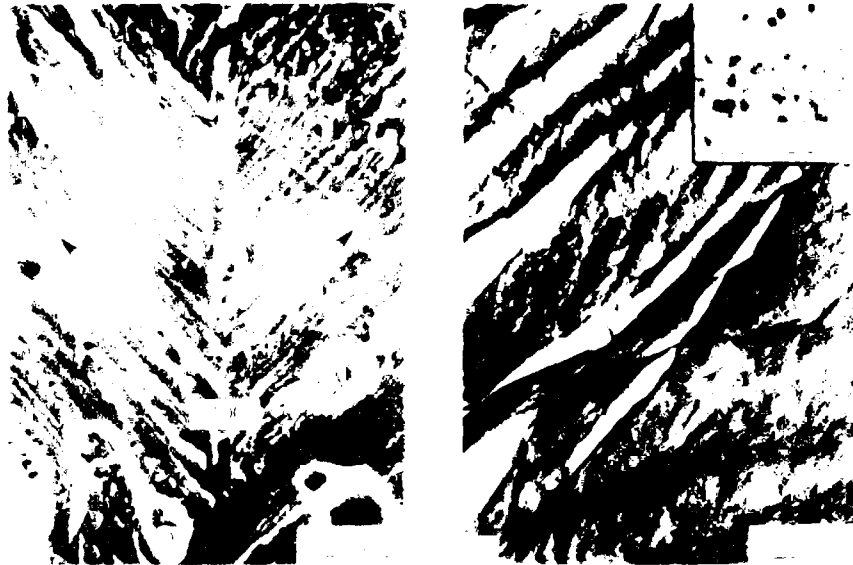


Figure 12. Optical micrographs showing crack surfaces of a peak-aged Al-In-Mg single crystal after rapid cracking ( $\sim 10$  mm/s) in distilled water. The crack is perpendicular to the cleavage plane. The inset in the upper right corner shows a magnified view of the crack surface.

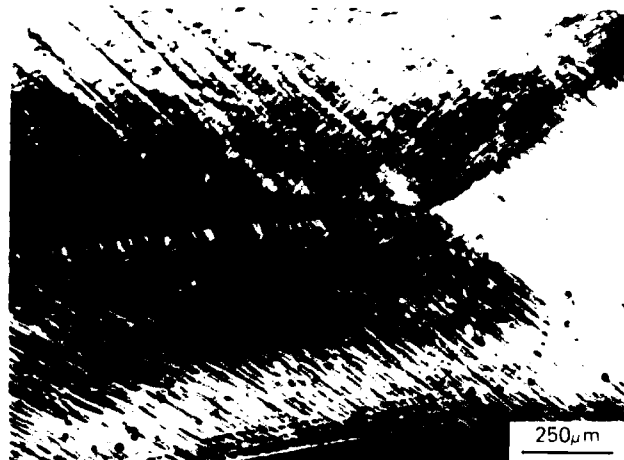


Figure 13. Optical micrograph showing slip around  $\{100\}$  cleavage-plane crack on the side surface of a peak-aged Al-In-Mg single crystal after rapid cracking ( $\sim 10$  mm/s) in distilled water.

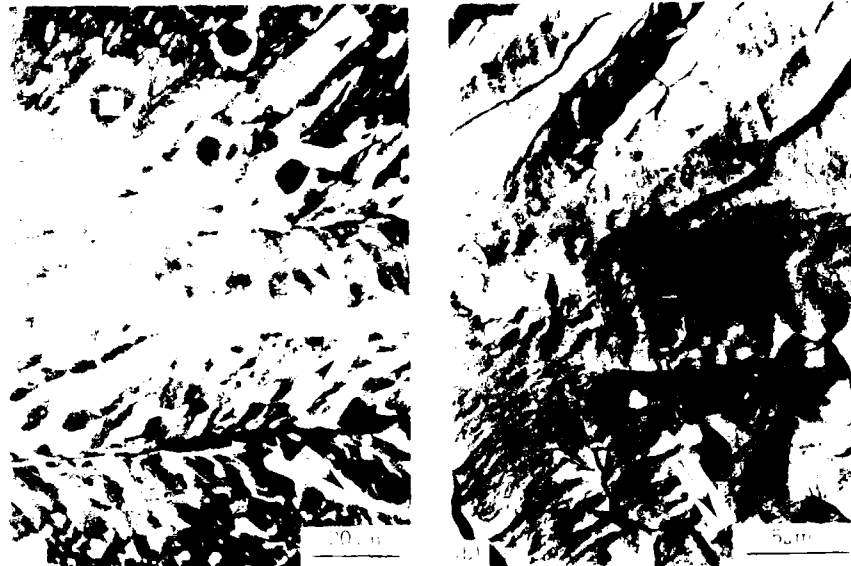


Figure 14. (a) 10 $\mu$ m and (b) 5 $\mu$ m of cleavage-like fracture surface of slow crack growth (10 $\mu$ m) Al-Zn-Mg single crystal. The cleavage-like fracture surface is composed of many cleavage-like surfaces with a high degree of orientation. The cleavage-like fracture surface is composed of many cleavage-like surfaces with a high degree of orientation. The cleavage-like fracture surface is composed of many cleavage-like surfaces with a high degree of orientation.

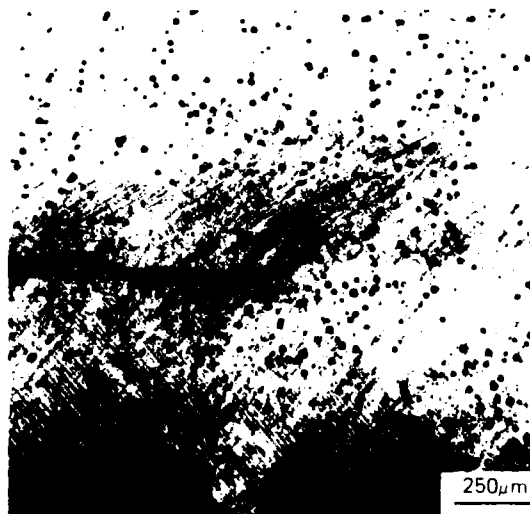


Figure 15. Optical micrograph showing slip around (100) cleavage-like crack in the interior of a peak-hard (HV-150) Al-Zn-Mg single crystal after slow crack growth ( $\sim 10^{-3}$  mm/s) in water.

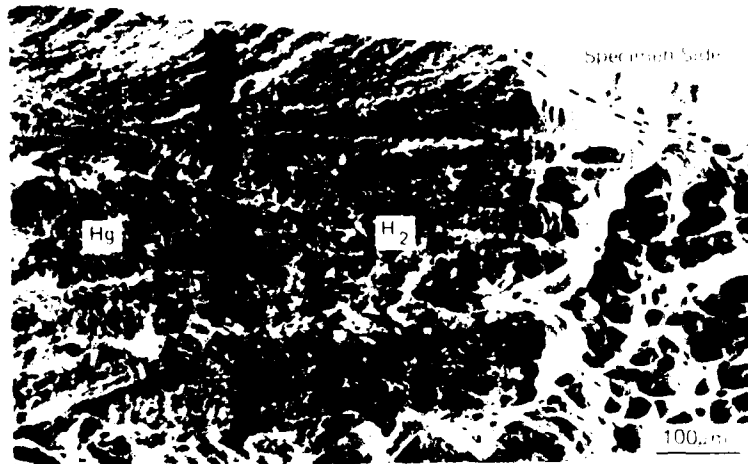


Figure 16. SEM of fracture surface profile in a near- $\langle 111 \rangle$  orientation, produced by rapid crack growth in pure copper in liquid mercury and then, after evaporating the mercury and annealing at 200°C, produce a striation, by rapid crack growth in pure copper in liquid mercury (101494), and finally by crack growth in air at 200°C.

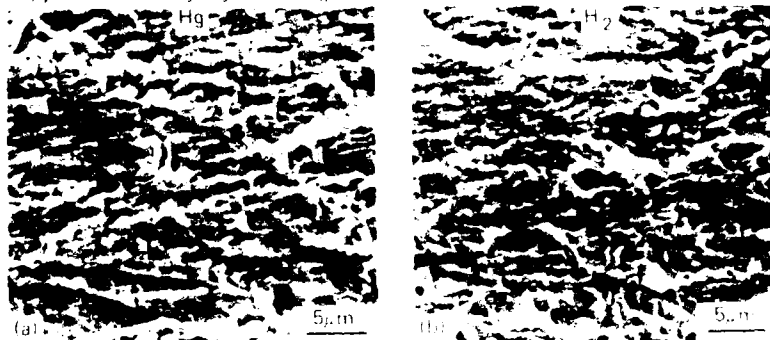


Figure 17. SEM of areas of the fracture surface in a near- $\langle 111 \rangle$  orientation, showing magnification, showing remnant of the striation produced by rapid crack growth in liquid mercury, and in air at 200°C.

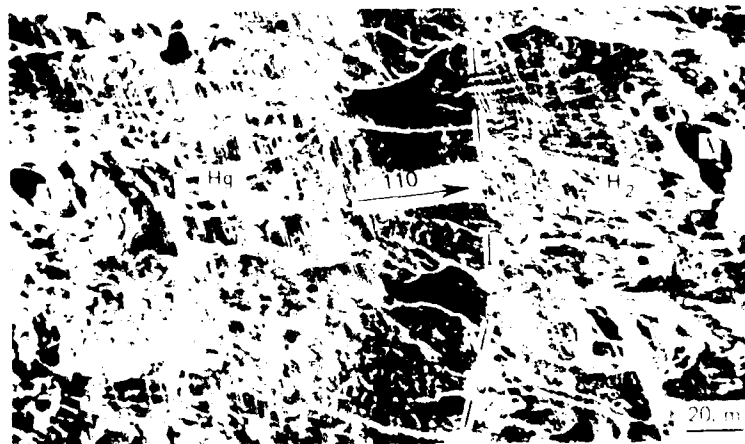


Figure 18. SEM of fracture surface profile in a near- $\langle 100 \rangle$  orientation, produced by rapid crack growth in pure copper in liquid mercury and then rapid crack growth in pure copper in liquid mercury (101494), showing steps, isolated large dimples (A), and striations.

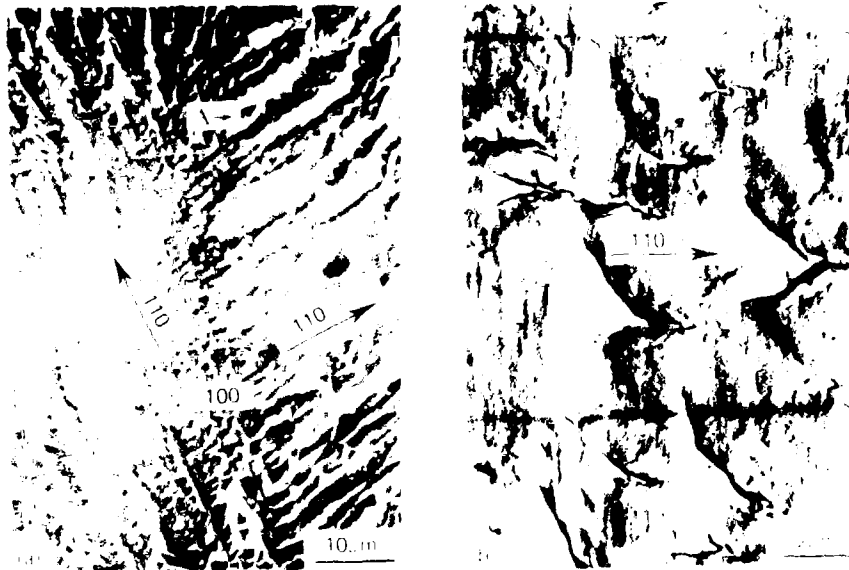


Figure 19. (a) SEM and (b) TEM micrographs of the surface of a nickel single crystal, with a tear ridge, after a tensile test at  $10^{-3}$  mm/s in gaseous  $H_2$  gas, at  $10^{-4}$  Pa, at 20°C. The slip lines are formed during a thermocycle process, and the tear ridge is formed during the final slip lines (110 and 110) slip lines, and the tear ridge is formed during the final slip lines.

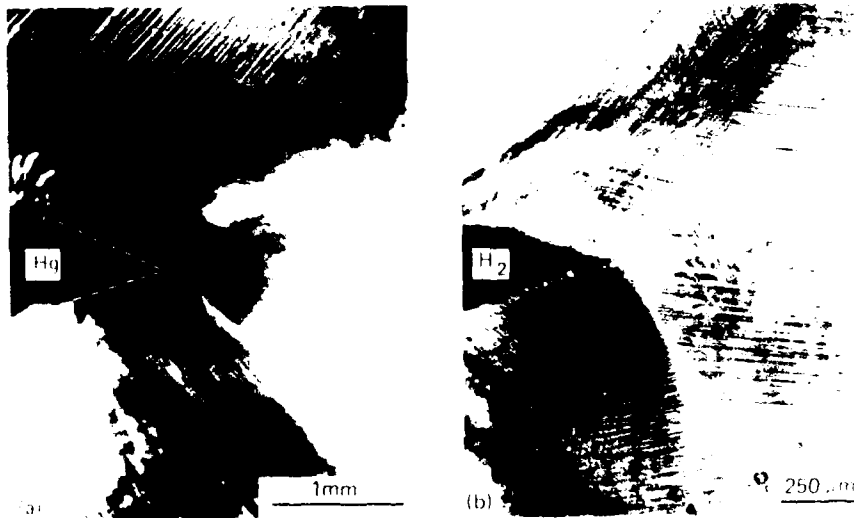


Figure 20. Optical micrographs showing extensive slip around cracks on the side surfaces of nickel single crystals cracked (a) rapidly (10 mm/s) in liquid mercury, and (b) slowly ( $10^{-3}$  mm/s) in gaseous hydrogen ( $10^{-4}$  Pa), at 20°C.

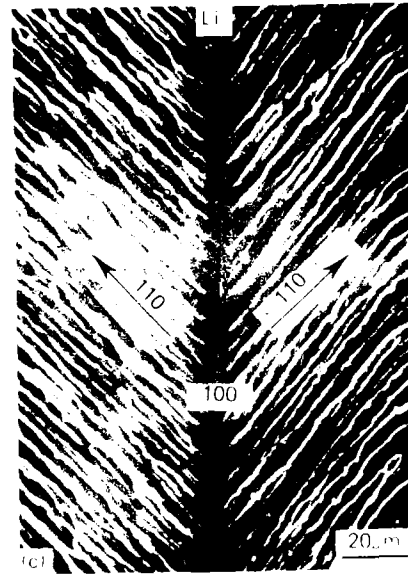
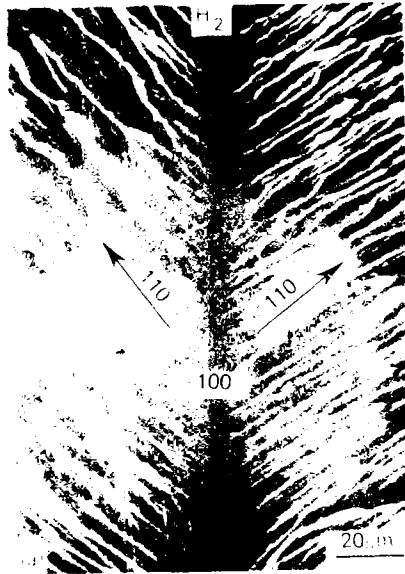


Figure 21. (a) SEM of cleavage facets fracture surface post-test in Fe-17Li (low nitrogen density alloy) showing a growth of  $\alpha$ -Fe phase in grain boundary region (100), (110), and (111) major planes growth along with liquid film between facets, showing step-like pattern, and low magnification SEM of step-like fracture surface at high magnification.



Figure 22. TEM of fracture surface produced in Fe-Si single crystal by slow crack growth ( $\sim 10^{-7}$  mm/s) in hydrogen, showing closely spaced slip lines and small depressions.



Figure 23. Optical micrograph showing extensive slip around cleavage-like crack on the side surface of a Fe-Si single crystal after rapid crack growth ( $\sim 1$  mm/s) in liquid indium at  $-160^{\circ}\text{C}$ .

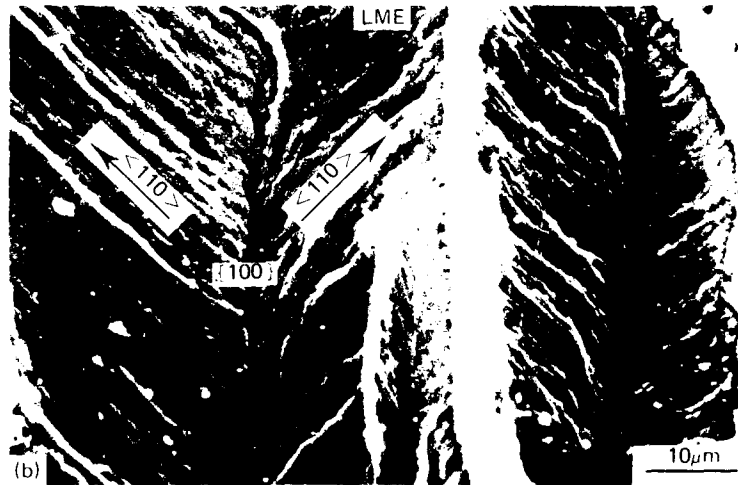
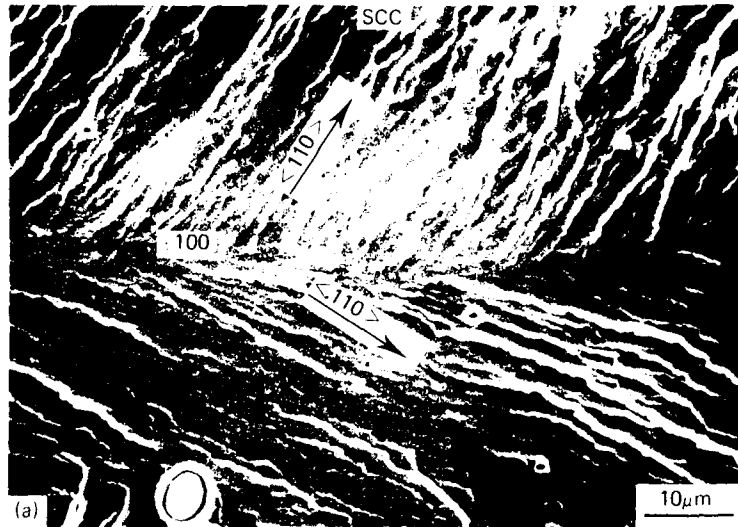
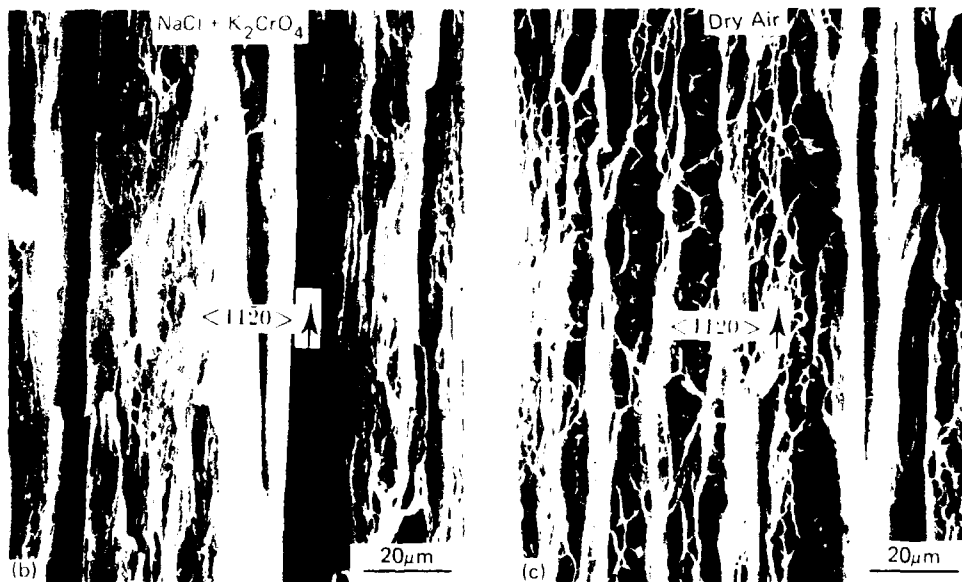
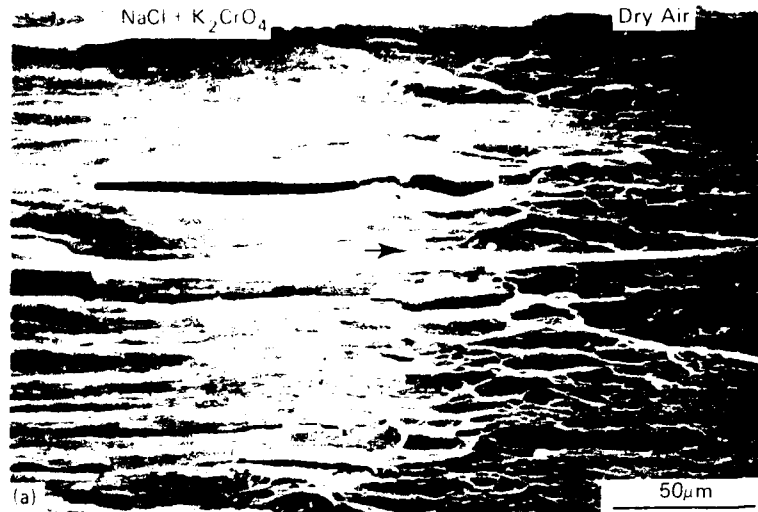


Figure 24. SEM of fracture surfaces produced in  $\beta$ -brass single crystals by (a) slow crack growth ( $\sim 10^{-3}$  mm/s) in distilled water at  $20^\circ\text{C}$ , and (b) rapid crack growth ( $\sim 10$  mm/s) in liquid gallium at  $-30^\circ\text{C}$ , showing herringbone patterns.



**Figure 25.** (a) SEM of fracture surface produced in a magnesium crystal by rapid crack growth ( $\sim 10$  mm/s) in a 3.3% NaCl + 2% K<sub>2</sub>CrO<sub>4</sub> environment and then by rapid crack growth in dry air, (b) and (c) areas of fracture surface at a higher magnification than in (a), showing shallow flutes/dimples and secondary cracks in areas produced in the salt solution and large, deep flutes/dimples in areas produced in dry air.



Figure 26. TEM of fracture surface produced in a magnesium crystal by rapid crack growth ( $\sim 10$  mm/s) in the aqueous environment, showing fluted/dimpled area (A) and cleavage-like area (B). The latter exhibits tongues associated with twins.

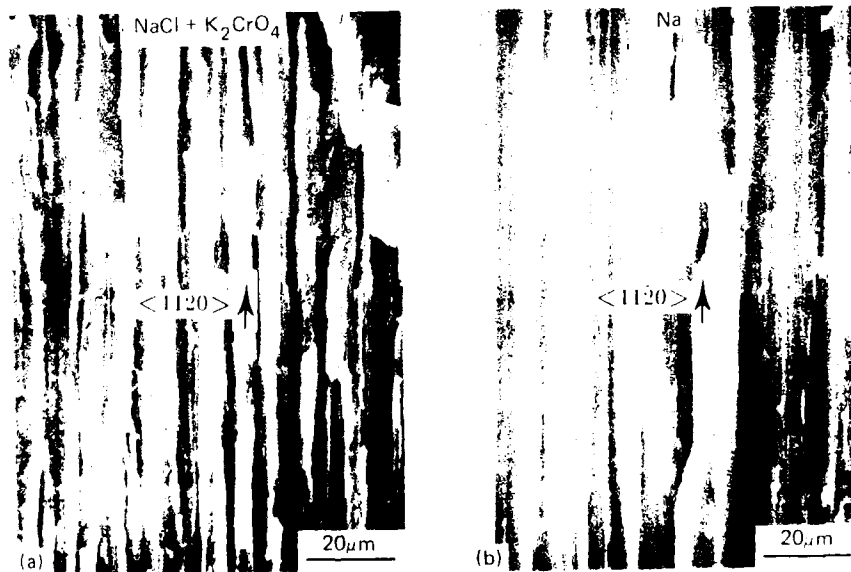


Figure 27. SEM of fracture surfaces produced in magnesium crystals by (a) slow crack growth ( $\sim 6 \times 10^{-4}$  mm/s) in 3.3% NaCl + 2%  $K_2CrO_4$  solution at 25°C, and (b) rapid crack growth ( $>10$  mm/s) in liquid sodium metal, showing shallow flutes on pyramidal planes.



**Figure 28.** SEM of fracture surfaces produced in magnesium crystals by (a) slow crack growth ( $\sim 3 \times 10^{-4}$  mm/s) in 3.3% NaCl + 2% K<sub>2</sub>CrO<sub>4</sub> solution at 20°C, and (b) rapid crack growth ( $>10$  mm/s) in liquid caesium at -50°C, showing cleavage-like fracture on basal planes.

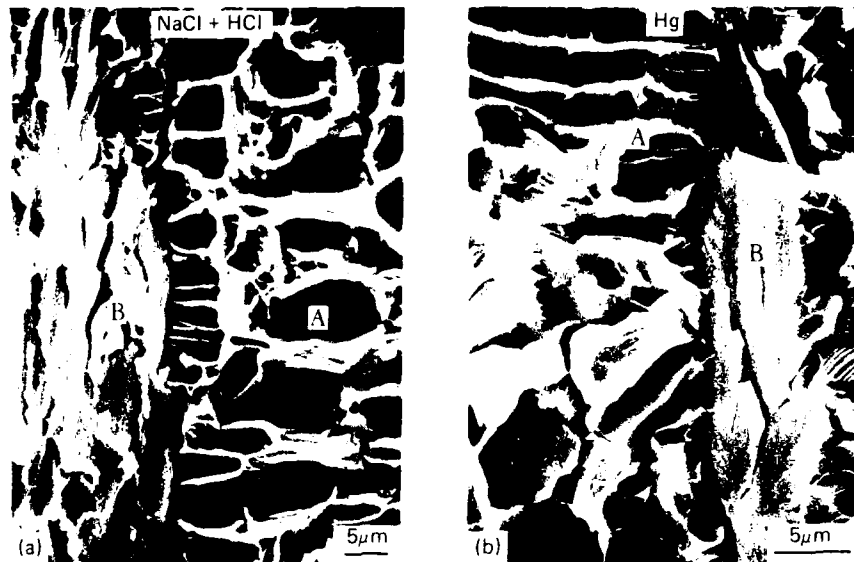
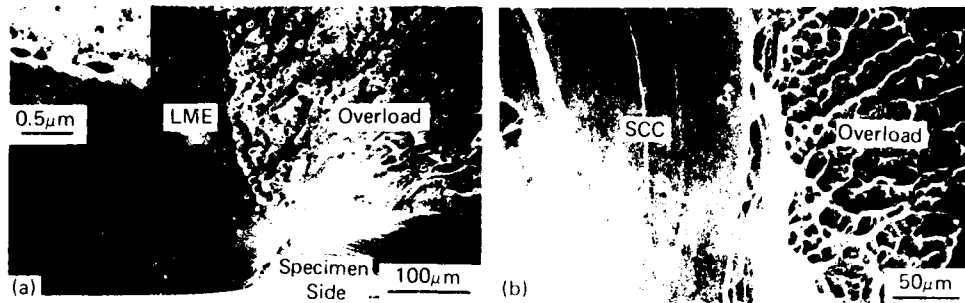


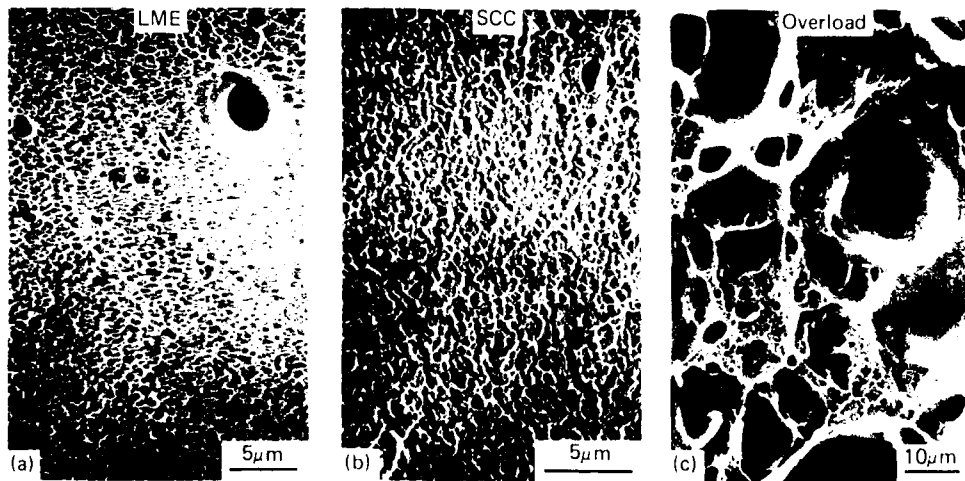
Figure 29. SEM of fracture surfaces produced in Ti 6Al 4V alloy by (a) crack growth ( $\sim 10^{-1}$  mm/s) in a 3.5% NaCl + 1M HCl environment at 20°C, and (b) rapid crack growth ( $>10$  mm/s) in liquid mercury at 20°C, showing fluted regions (A) and cleavage-like facets (B).



Figure 30. TEM of fracture surface produced in Ti 6Al 4V alloy by SCC in the aqueous environment, showing tear ridges and small, shallow dimples on cleavage-like areas, and fluted region (B).



**Figure 31.** SEM of fracture surfaces produced in Al-Zn-Mg bicrystals by (a) rapid crack growth ( $\sim 10$  mm/s) in the liquid eutectic at  $60^\circ\text{C}$  and then in dry air, and (b) slow crack growth ( $\sim 10^{-4}$  mm/s) in distilled water and then by rapid fracture in dry air at  $20^\circ\text{C}$ , showing transitions from 'brittle' intercrystalline to 'ductile' intercrystalline fracture. Inset is a TEM of a thin foil showing the grain-boundary microstructure.



**Figure 32.** SEM of areas of fracture surfaces shown in figure 31 at a higher magnification: (a) small dimples on LME area, (b) small dimples on SCC area, and (c) large, deep dimples, with small dimples within and between large dimples, on overload area.



Figure 33. SEM of fracture surfaces produced in 7075-T651 aluminum alloy by (a) slow crack growth ( $\sim 7^{-7}$  mm/s) in moist air (20% Relative Humidity), and (b) slow crack growth ( $\sim 10^{-7}$  mm/s) in solid indium, at 20°C, showing tear ridges and isolated small dimples on intercrystalline facets.

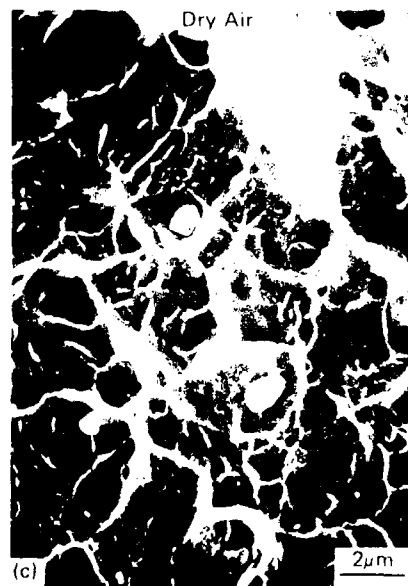
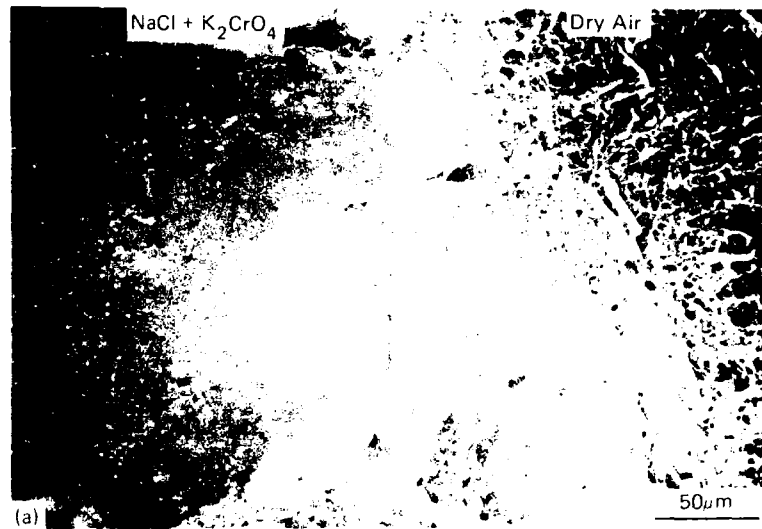


**Figure 34.** (a) SEM of intercrystalline fracture surface produced in magnesium by rapid crack growth ( $\sim 10$  mm/s) in 3.3%NaCl + 2%K<sub>2</sub>CrO<sub>4</sub> solution and then by overload in dry air at 20°C, showing transition from 'brittle' intercrystalline to 'ductile' intercrystalline fracture: (b) and (c) SEM of 'brittle' and 'ductile' areas, respectively, showing small dimples and relatively smooth areas produced by crack growth in the salt solution, and large dimples, with small dimples within large dimples, produced by crack growth in dry air.



Figure 35. TEM of intercrystalline fracture surface produced in magnesium by rapid crack growth in the aqueous environment, showing closely spaced slip lines (A), shallow flutes (B), and small dimples (C), not resolved by SEM.

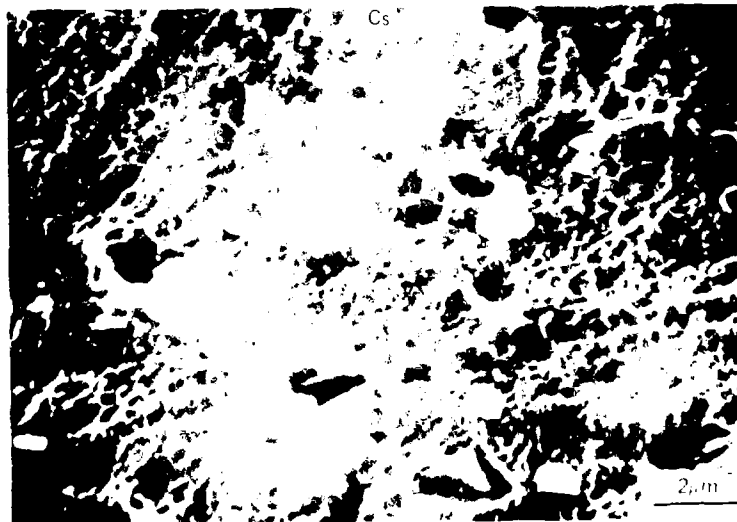
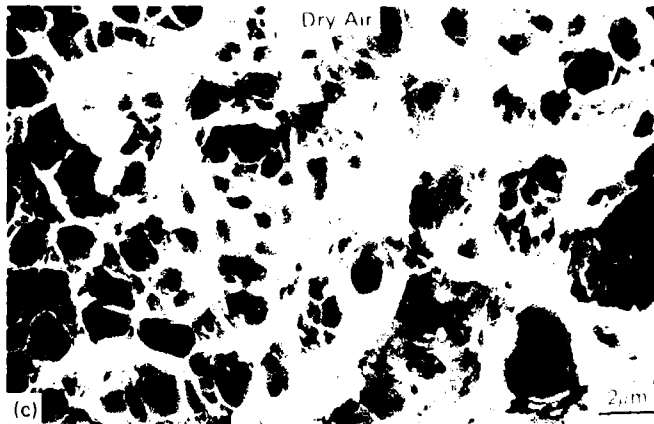
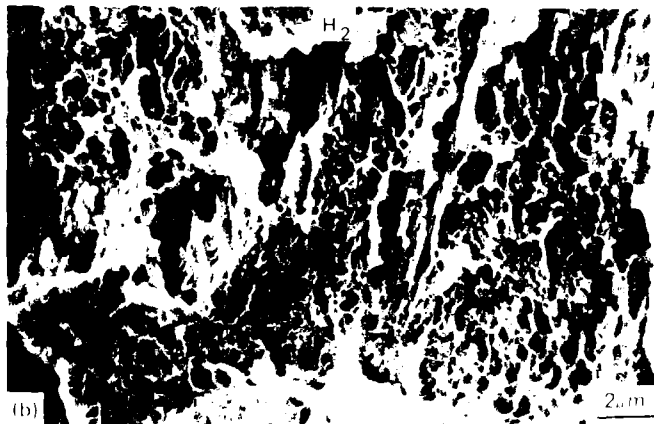
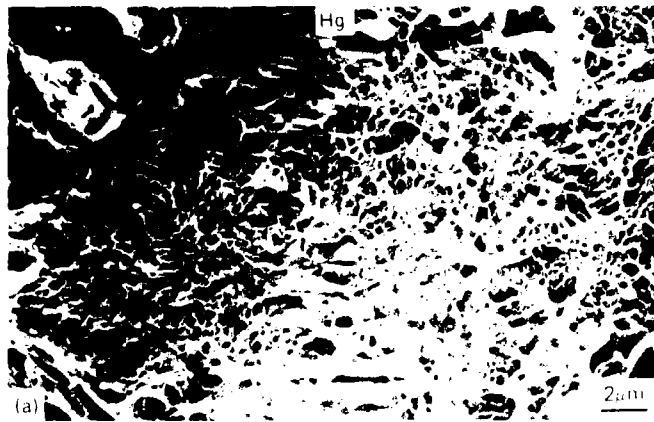
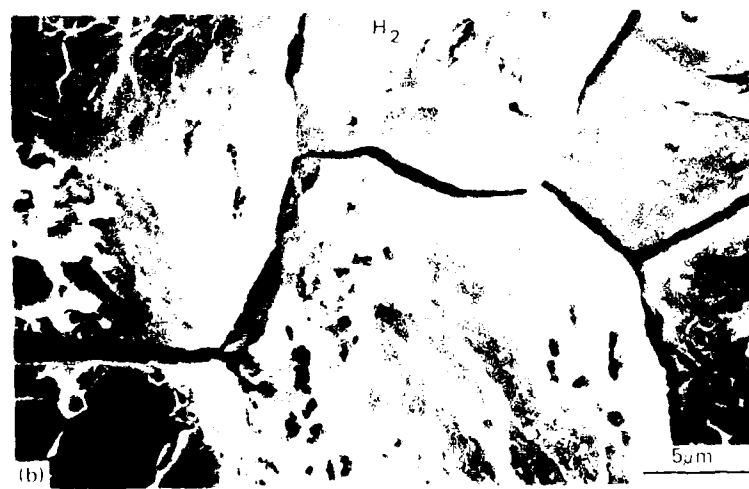


Figure 36. SEM of intercrystalline fracture surface produced in magnesium by rapid crack growth (10 mm/s) in lipid environment, showing small dimples.



**Figure 37.** SEM of fracture surfaces produced in D9a1 steel (temporal at 290°C (HV-570) by (a) rapid crack growth ( $>10$  mm/s) in liquid mercury, (b) crack growth ( $\sim 10^{-2}$  mm/s) in gaseous hydrogen (101 kPa), and (c) overload fracture in air, at 20°C. Dimples are generally smaller and shallower after HAC and LME than after overload.



**Figure 38.** SEM of fracture surfaces produced in D9ac steel tempered at 400°C (HV-50) by (a) rapid crack growth ( $>10$ mm/s) in liquid mercury, and (b) crack growth ( $\sim 10^{-2}$  mm/s) in gaseous hydrogen (101kPa, at 10°C), showing tear ridges and isolated dimples on 'brittle' intercrystalline facets.

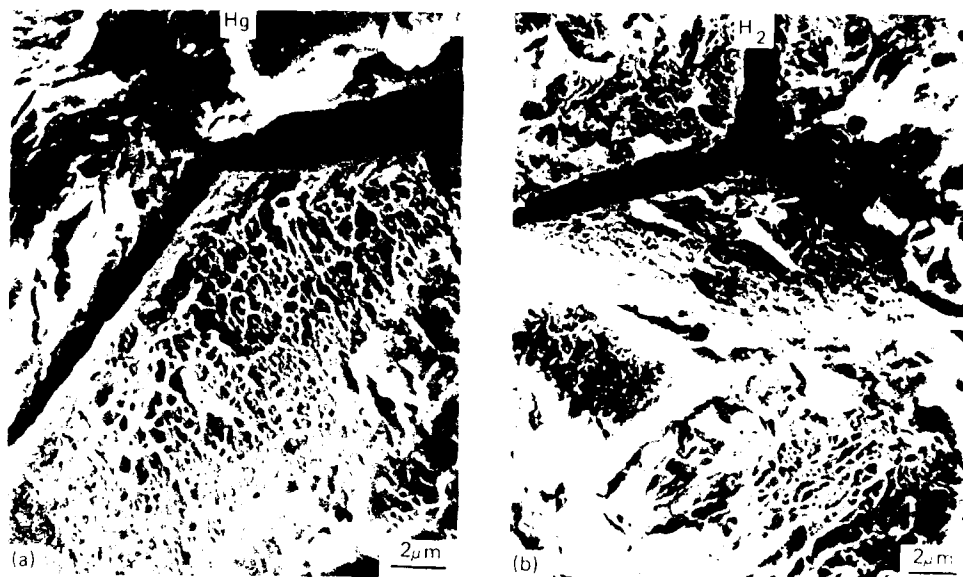


Figure 39. SEM of fracture surfaces produced in 0640 steel tempered at 550°C (HV=400) by (a) rapid crack growth ( $>10$  mm/s) in liquid mercury, and (b) crack growth ( $\sim 10^{-2}$  mm/s) in gaseous hydrogen (0.1 MPa) at 20°C, showing dimpled intercrystalline facets.



Figure 40. SEM of fracture surface produced in 0640 steel tempered at 200°C by rapid cracking in liquid mercury, showing very small dimpled facets (area A) which were not resolved by SEM, as well as areas of clearly defined dimples on intercrystalline facets.



Figure 11. SEM of fracture surface produced by cyclic bending of a 2024-T3 aluminum specimen. The fatigue crack growth is characterized by the presence of fatigue striations. The overload fracture is characterized by the presence of a rough, irregular surface. The fatigue crack growth is characterized by the presence of fatigue striations. The overload fracture is characterized by the presence of a rough, irregular surface. The fatigue crack growth is characterized by the presence of fatigue striations. The overload fracture is characterized by the presence of a rough, irregular surface.



Figure 12. SEM of fracture surface produced by cyclic bending of a 2024-T3 aluminum specimen. The fatigue crack growth is characterized by the presence of fatigue striations. The stretched zone is characterized by the presence of a smooth surface. The overload fracture is characterized by the presence of a rough, irregular surface. The fatigue crack growth is characterized by the presence of fatigue striations. The stretched zone is characterized by the presence of a smooth surface. The overload fracture is characterized by the presence of a rough, irregular surface.

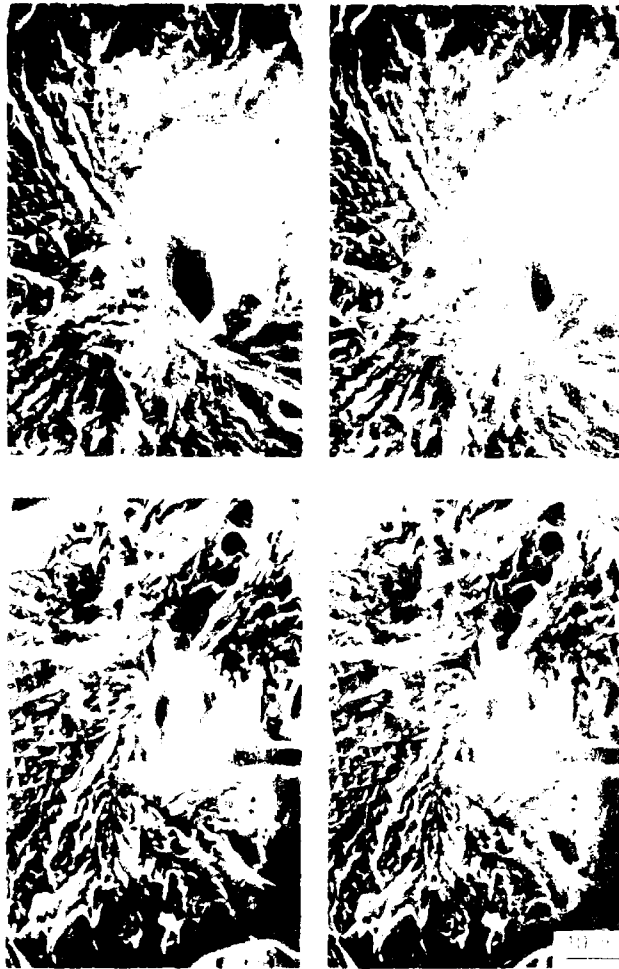


Figure 39. Scanning electron micrographs of the surface morphology of the material. The top two images show a relatively smooth surface with some small, dark, circular features. The bottom two images show a more textured surface with larger, irregular, and interconnected features, possibly representing a different stage of growth or a different material composition. A scale bar is visible in the bottom right corner of the fourth image.

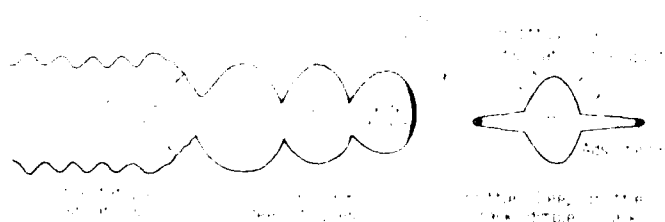


Figure 40. Schematic diagrams illustrating the morphology of a material. The left diagram shows a series of interconnected, rounded, and elongated structures, resembling a chain of beads or a porous network. The right diagram shows a single, elongated, and somewhat flattened structure with a central constriction, possibly representing a different morphological form or a cross-section of the material.

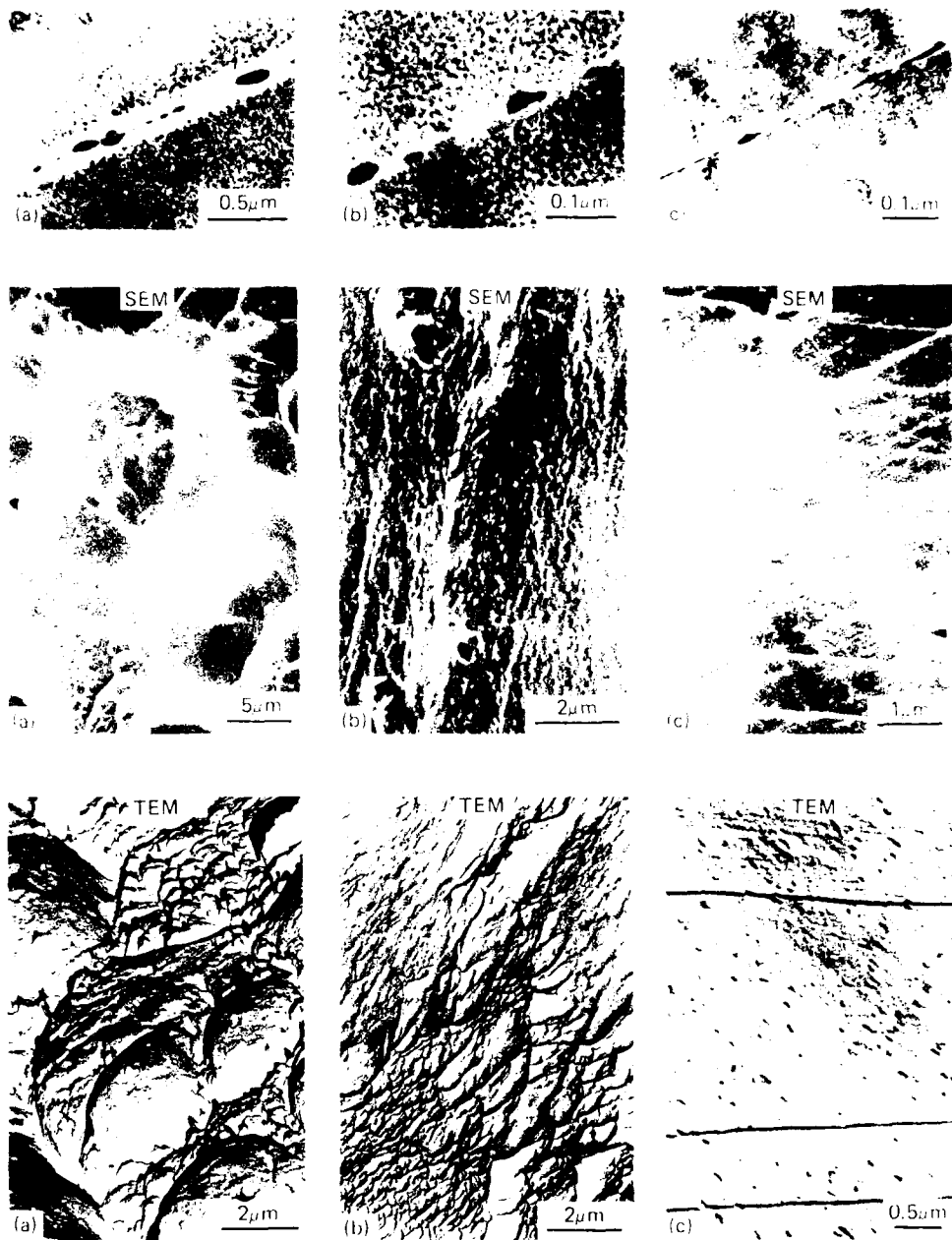
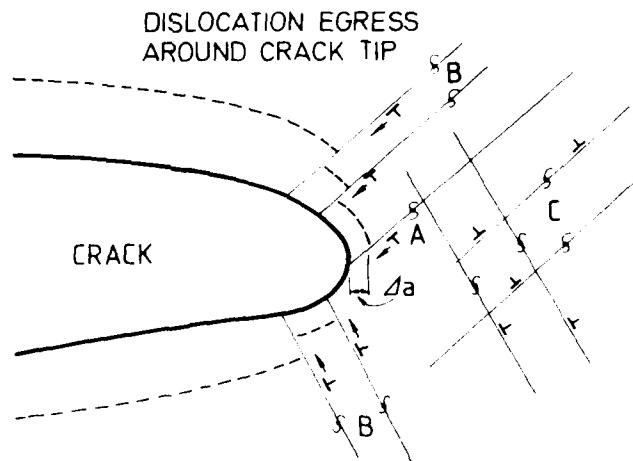
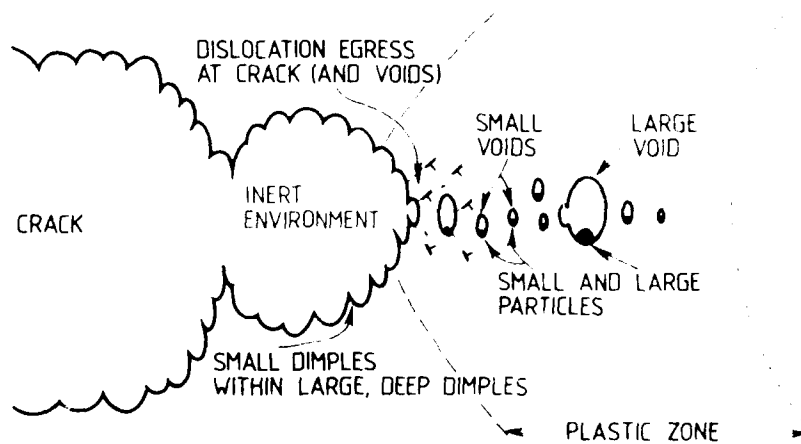


Figure 45. SEM and TEM of intercrystalline fracture surfaces produced by overload fracture in dry air at 20°C in Al-Zn-Mg bicrystals with (a) wide precipitate-free zone (PFZ) and widely spaced grain-boundary precipitates (GBP), (b) narrow PFZ and more closely spaced GBP, and (c) very narrow PFZ and even more closely spaced GBP. Dimples of various sizes and depths are evident in (a) and (b), but only fine slip lines and impressions of precipitates are clearly visible in (c). Note that the magnifications are different in (a), (b), and (c).



**Figure 46.** Schematic diagram illustrating the mechanism of ductile crack growth: Egress of dislocations nucleated from near-crack-tip sources (A) **exactly** on planes intersecting crack tips produce an increment of crack advance,  $\Delta a$ , but dislocations emanating from sources (B) and (C) produce only opening or contribute to the general strain ahead of cracks. In other words, most dislocations produce crack blunting rather than crack growth. (Dislocation nucleation from crack tips does **not** occur to a significant extent).



**Figure 47.** Schematic diagram showing the fracture surface and crack-tip profiles, and distribution of voids ahead of ductile cracks growing predominantly by egress of dislocations around crack tips. Considerable blunting occurs at crack tips and large strains develop ahead of cracks so that extensive void nucleation and growth occurs ahead of cracks, especially around the larger particles. Large, deep dimples with small, shallow dimples within them are therefore produced on fracture surfaces.

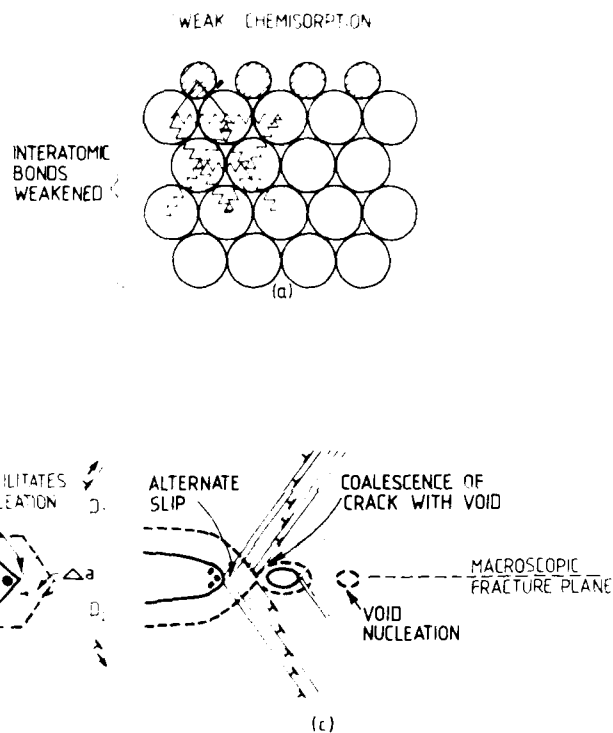
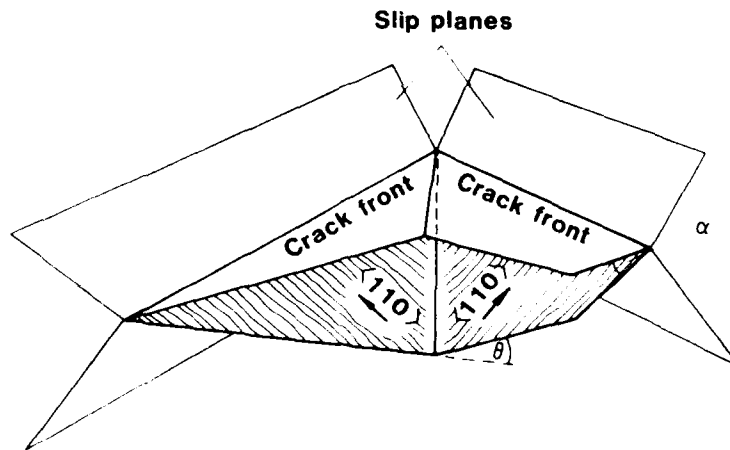
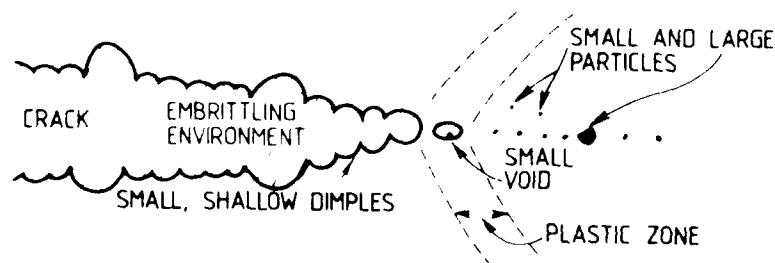


Figure 48. Schematic diagrams illustrating the adsorption-induced localized-slip process for environmentally assisted cracking: (a) Adsorbed metal or hydrogen atoms (and possibly hydrogen atoms in the first few atomic layers) weaken interatomic bonds and thereby facilitate the shear movement of atoms (i.e. dislocation nucleation) at crack tips, (b) dislocation injection from the crack tip first on plane  $D_1$  and then on plane  $D_2$  produces an increment of crack advance,  $a$ , and (c) some dislocation activity (not shown) occurs ahead of cracks producing voids, and cracks growing by alternate-slip coalesce with voids so that the macroscopic fracture plane bisects the active slip planes. Crack fronts are also parallel to the line of intersection of slip planes with the crack plane - see figure 49.



**Figure 49.** Diagram illustrating the formation of herringbone patterns on fracture surfaces of fcc and bcc materials [54]. Crack growth occurs in two  $\langle 110 \rangle$  directions, and involves different slip systems, on either side of a central spine. The fracture surfaces on either side of the spine are tilted with respect to each other, and the tilt angle,  $\alpha$ , is geometrically related to the crack-tip-opening angle,  $\lambda$ . ( $\tan \alpha/2 = \tan \lambda/2 \cdot \cos 45^\circ$ ) Crack growth by an alternate-slip mechanism requires the crack faces to rotate about a  $\langle 110 \rangle$  (crack-front) axis and, when cracks in adjacent areas grow in two mutually orthogonal directions, this can only occur if the crack front breaks up into small segments separated by steps. These steps, parallel to the directions of crack growth on either side of the spine, are responsible for the herringbone patterns.



**Figure 50.** Schematic diagram showing the fracture-surface and crack-tip profile, and distribution of voids ahead of 'brittle' cracks growing predominantly by injection of dislocations from crack tips. Compared with ductile cracks (Fig. 47), less blunting occurs at crack tips, strains ahead of cracks are lower, and voids are formed only just ahead of cracks. Small, shallow dimples are therefore produced on fracture surfaces.

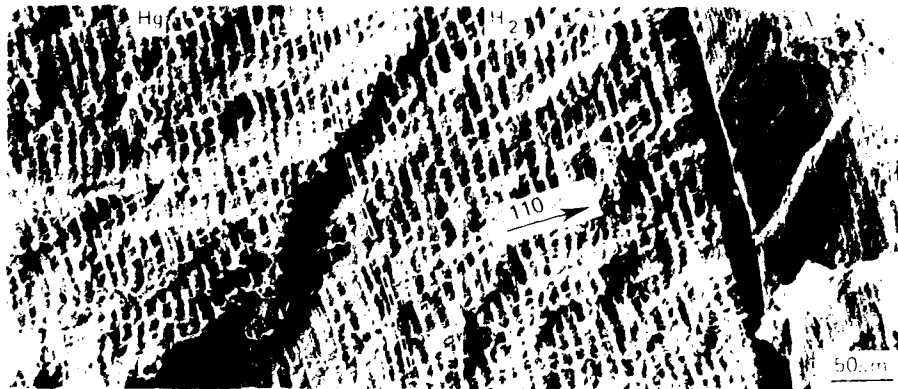


Figure 51. SEM of fracture surface produced in a nickel single crystal by fatigue crack growth in  $H_2$ ,  $H_2O$  in liquid mercury and then, after completely evaporating the mercury from the crack, in argon, argon at 100 kPa, and then in argon. Brittle striations and dimples are produced in mercury and hydrogen environments, whereas ductile striations are produced in inert environments.

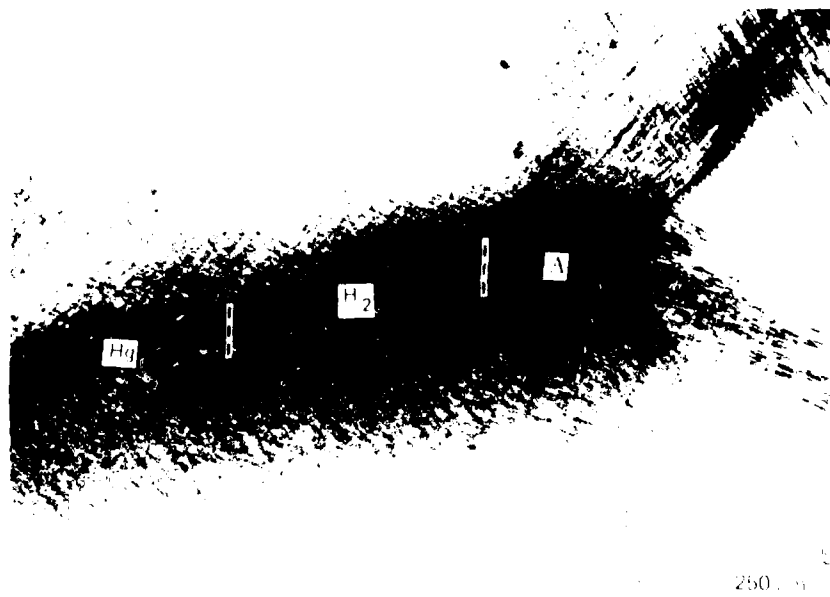


Figure 52. Optical micrograph of a specimen section of a nickel single crystal after fatigue crack growth in  $H_2$ ,  $H_2O$  in liquid mercury and then, after evaporating the mercury from the crack, in argon at 100 kPa, and then in argon. The more extensive fatigue striations are formed after fatigue in mercury and hydrogen environments, whereas they are more intense and extensive after fatigue in argon.

**DISTRIBUTION**

**AUSTRALIA**

Department of Defence

Defence Central

Chief Defence Scientist  
Deputy Chief Defence Scientist (shared copy)  
Superintendent, Science and Program Administration (shared copy)  
Controller, External Relations, Projects and  
Analytical Studies (shared copy)  
Counsellor, Defence Science (London) (Doc Data Sheet Only)  
Counsellor, Defence Science (Washington) (Doc Data Sheet Only)  
Defence Central Library  
Document Exchange Centre, DISB (18 copies)  
Joint Intelligence Organisation  
Librarian H Block, Victoria Barracks, Melbourne  
Director General - Army Development (NSO) (4 copies)

Aeronautical Research Laboratories

Director  
Library  
Superintendent - Aircraft Materials  
Divisional File - Aircraft Materials  
W.J. Pollock  
F. Rose  
N. Goldsmith  
B. Hinton  
N. Ryan  
Authors: S. Lynch

Materials Research Laboratories

Director/Library

Defence Research Centre

Library

RAN Research Laboratory

Library

Navy Office

Navy Scientific Adviser

Army Office

Scientific Adviser - Army

Air Force Office

Air Force Scientific Adviser  
Aircraft Research and Development Unit  
Library  
Technical Division Library  
HQ Support Command (SLENGO)  
RAAF College, Point Cook

Government Aircraft Factories  
Library

Department of Aviation  
Library

Statutory and State Authorities and Industry  
Australian Atomic Energy Commission, Director  
CSIRO, Division of Materials Science, Library  
SEC of Vic., Herman Research Laboratory, Library  
BHP, Melbourne Research Laboratories  
Hawker de Havilland Aust. Pty Ltd, Bankstown, Library

Universities and Colleges

Adelaide  
Barr Smith Library  
Prof R. Miller

Flinders  
Library

Meibourne  
Engineering Library

Monash  
Hargrave Library  
Prof I.J. Poimear, Materials Engineering

Newcastle  
Dr J.A. Lewis, Mechanical Engineering

NSW  
Head, Metallurgy Dept

Queensland  
Library

RMIT  
Library

Wollongong  
Prof w.J. Plumbridge

**CANADA**

Energy Mines & Resources Dept  
Physics and Metallurgy Research Laboratories

Universities and Colleges

Saskatchewan  
Prof I LeMay

**FINLAND**

Technical Research Centre of Finland, Metals Laboratory  
Dr H. Hanninen

**FRANCE**

ONERA, Library

**GERMANY**

Universities and Colleges

Max-Planck-Institut fur Eisenforschung GmbH  
Prof Dr Peter Meumann  
Dr Horst Vehoff (shared copy)

Erlangen-Nurnberg  
Prof H. Mughrabi, Institute fur Werkstoffwissenschaften

Universitaat des Saarlandes  
H. Gleiter

**INDIA**

CAARC Coordinator Materials  
National Aeronautical Laboratory, Information Centre

**INTERNATIONAL COMMITTEE ON AERONAUTICAL FATIGUE**  
per Australian ICAF Representative (25 copies)

**JAPAN**

National Aerospace Laboratory

**NETHERLANDS**

National Aerospace Laboratory (NLR)  
Dr R.J.H. Wanhill  
Library

**NEW ZEALAND**

Defence Scientific Establishment, Library

**SWEDEN**

Aeronautical Research Institute, Library

## UNITED KINGDOM

CAARC, Secretary  
Royal Aircraft Establishment  
Farnborough, Dr G. Wood, Materials Department  
Admiralty Research Establishment  
St Leonard's Hill, Superintendent  
National Physical Laboratory  
Dr M.P. Seah  
Library  
National Engineering Laboratory, Library  
Brisith Library, Document Supply Centre  
Alcan International Laboratories  
Dr N.J.H. Holroyd  
Dr G.M. Scamans (shared copy)  
Fulmer Research Institute Ltd, Research Director  
Rolls-Royce Ltd, Aero Division Bristol, Library  
Welding Institute, Library  
Atomic Energy Research Establishment  
Dr R Bullough  
Dr M.W. Finnis (shared copy)  
P Trevena  
M. Nicholas (shared copy)

### Universities and Colleges

Cambridge  
Dr J.F. Knott, Dept of Met. & Mat. Science  
Library, Engineering Department  
  
Cranfield Inst. of Technology  
Library  
  
Leeds  
Dr J.D. Souly, Metallurgy  
  
Manchester  
Dr R Newman, Corrosion & Protection Centre  
Prof E. Smith, Metallurgy  
  
Newcastle upon Tyne  
Prof R.N. Parkins  
  
Open  
Prof C.N. Reid

## UNITED STATES OF AMERICA

NASA Scientific and Technical Information Facility  
Materials Information, American Society for Metals  
The Chemical Abstracts Service  
McDonnell Aircraft Company, Library  
Battelle Columbus Laboratories, Dr A.J. Markworth  
Battelle Pacific Northwest Laboratories, Dr R.H. Jones

Los Alamos National Laboratory, Dr J.E. Hack  
Sandia National Laboratory  
Dr M. Baskes  
Murray S. Daw (shared copy)  
Brookhaven National Laboratory, Dr Karl Sieradzki  
Oak Ridge National Laboratory, Dr S. Michael Ohr  
General Electric Company, Dr Clyde Briant  
Alcoa Laboratories, Dr A.K. Vasudevan  
Naval Research Laboratory, Washington  
C.D. Beachem  
D.A. Meyn (shared copy)  
G. Yoder (shared copy)  
Martin Marietta Laboratories  
Dr A.R.C. Westwood  
Dr J.R. Pickens (shared copy)  
National Bureau of Standards  
Dr N. Pugh  
Dr R Thomson  
Benet Weapons Laboratory, Dr M. Kamdar

Universities & Colleges

Brown  
Prof S. Suresh, Engineering

California  
Prof R.O. Ritchie, Mat. Sci. & Mineral Eng.

Carnegie-Mellon  
Prof I.M. Bernstein, Metallurgy & Mat. Science  
Prof A.W. Thompson, Metallurgy & Mat. Science (shared copy)

Harvard  
Prof J.R. Rice, Divn. of Applied Sciences

Illinois  
Prof R.K. Birnbaum, Metallurgy and Mining Engineering  
Dr I.M. Robertson, Metallurgy and Mining Engineer. (shared copy)

Illinois Inst. of Tech.  
Prof P. Gordon, Metallurgical and Materials Engineering

Iowa  
Prof R.I. Stephens

Lehigh  
Prof R.P. Wei

Massachusetts Inst. of Tech.  
Dr Mark Eberhart  
Prof R.M. Latanision  
MIT Libraries

Michigan Technological  
Dr L.A. Heidt, Metallurgical Engineering

Minnesota

Prof R.A. Oriana, Chem. Eng. & Mat. Science  
Prof W.W. Gerberich, Chem. Eng. & Mat. Science (shared copy)

Ohio State

Prof J.P. Hirth, Metallurgical Engineering

Pennsylvania

Prof C.J. McMahon, Mat. Sci & Engineering  
Prof Campbell Laird, Mat. Sci & Engineering (shared copy)

Rensselaer Polytechnic Institute

Prof N. Stoloff, Materials Engineering  
Prof D.J. Duquette, Materials Engineering (shared copy)

Rochester

Prof S.J. Burns, Mechanical Engineering

Virginia Polytechnic Institute

Prof M.K. Louthan Jr, Materials Engineering

SPARES (20 copies)

TOTAL (179 copies)

Department of Defense  
DOCUMENT CONTROL DATA

1a. Alt No. AR-004-516	1b. Establishment No. ARL-MAT-R-119	2. Document Date DECEMBER 1986	3. Task No. DST 44-049
4. Title ENVIRONMENTALLY ASSISTED CRACKING: OVERVIEW OF EVIDENCE FOR AN ADSORPTION-INDUCED LOCALISED-SLIP PROCESS		5. Security a. Document UNCLASSIFIED	6. No. Pages 49
5. Author(s) S. P. LYNCH		b. Title c. Abstract U U	7. No. Refs. 102
		9. Downgrading Instructions -	

10. Originator, Author and Address

Aeronautical Research Laboratories  
P.O. Box 4331,  
MELBOURNE, VIC. 3001

11. Authority for downgrading  
a. Sponsor b. Security c. Downgrading d. Approval

12. Security Distribution

Approved for public release

Where appropriate, outside stated limitations, should be referred to the AFOSI Defense Information Services Branch, Department of Defense, Campbelt Park, CANTON, MA 01901

For this document may be AFOSI/AFDD or other copies and awareness services available to you.

13. Limitations

13a. Limitation for other purposes (if any) (if any) may be (if any) restricted to

13b. Keywords	13c. Unavailable
Stress corrosion	Fractography
Fracture tests	Liquid metals
Hydrogen embrittlement	
Adsorption	
Dissipation (materials)	

14. Abstract

Metallographic and fractographic studies of crack growth in aluminium alloys, nickel, magnesium, titanium alloys & brass-iron-silicon, and high-strength steels in liquid-metal, aqueous, hydrogen, and inert environments are reviewed. Studies of transcrystalline cracking in single crystals are emphasized but some observations of intercrystalline cracking are also included. Remarkable similarities between hydrogen-assisted cracking, stress-corrosion cracking, and adsorption-induced liquid-metal embrittlement were observed for all the above materials. For a given material, not only was the detailed appearance of fracture surfaces similar but the crystallographic fracture planes and directions, and the active slip planes, were also the same for crack growth in the different embrittling environments. These and other similarities suggest that hydrogen-assisted

This paper is to be used to report information which is required by the Establishment for its own use but which will not be added to the OPI data base unless specifically requested.

16. Abstract

cracking and stress-corrosion cracking as well as liquid-metal embrittlement are due to adsorption at crack tips for the materials and conditions studied. Embrittlement of aluminium alloys, nickel, titanium alloys, and magnesium in aqueous or hydrogen environments was also observed at such high crack velocities (under certain conditions) that there was insufficient time for diffusion of hydrogen ahead of cracks, further supporting a mechanism based on adsorption (of hydrogen) at crack tips. The metallographic and fractographic observations showed that environmentally assisted cracking occurred by a more localised plastic-flow/microvoid-coalescence process than that which occurred in inert environments. Dislocation processes occurring during ductile and brittle fracture are discussed, and it is concluded that environmentally assisted cracking occurs because adsorption facilitates the injection of dislocations from crack tips and thereby promotes the coalescence of cracks with voids ahead of cracks. Recent high-voltage transmission-electron microscopy studies, surface-science observations, and theoretical work, which support an adsorption mechanism or a localised-slip mechanism for water for environmentally assisted cracking, are also reviewed.

17. Report

Aeronautical Research Laboratories, Melbourne

18. Management Series and Number  
AIRCRAFT MATERIALS  
SERIES 119

19. Cost Code  
55 1276

20. Type of Report and Period Covered

21. Group for Program - Act

22. Date of Report (month)

1976

END

DATE  
FILMED

11 87

DTIC